Sensors & Actuators: A. Physical 359 (2023) 114468

Contents lists available at ScienceDirect

Sensors and Actuators: A. Physical

journal homepage: www.journals.elsevier.com/sensors-and-actuators-a-physical

Review

Emerging 2D borophene: Synthesis, characterization, and sensing applications

Arifur Rahman [a,b,1], Md Tawabur Rahman [c,*,1], Mohammad Asaduzzaman Chowdhury [b], Saad Bin Ekram [c], M.M. Kamal Uddin [b], Md. Rasidul Islam [d], Liang Dong [e]

[a] Department of Mechanical Engineering, Bangabandhu Textile Engineering College, Kalihati, Tangail 1970, Bangladesh
[b] Department of Mechanical Engineering, Dhaka University of Engineering & Technology, Gazipur 1707, Bangladesh
[c] Department of Electrical and Electronic Engineering, Khulna University of Engineering & Technology (KUET), Khulna 9203, Bangladesh
[d] Department of Electrical and Electronic Engineering, Bangamata Sheikh Fojilatunnesa Mujib Science & Technology University, Jamalpur 2012, Bangladesh
[e] Iowa State University, Ames, IA 50011, USA

ARTICLE INFO

Keywords:
Borophene
Synthesis
Characterization
Sensors
2D nanomaterial
Healthcare
Applications

ABSTRACT

Borophene, a two-dimensional (2D) monolayer of elemental boron, has emerged as an intriguing material with superior characteristics including outstanding electronic, optical, chemical, mechanical, and catalytic properties. Due to superior properties, borophene has shown great prospects for a variety of novel applications in the field of energy storage devices, supercapacitors, sensors, and healthcare devices. This review provides an overview of various synthesis techniques to produce borophene nanostructures. Additionally, different simulation approaches have been discussed for studying the structural, electronic, and sensing properties of borophene and its composites. Besides synthesis, this review focuses on exploring the structural and morphological characteristics of borophene materials. Moreover, the uses of 2D borophene in gas sensing, humidity sensing, as well as other chemical sensing have been discussed. Lastly, the current challenges and prospects of this promising 2D nanomaterial have been extensively addressed.

1. Introduction

Boron is a light weight material and chemically versatile element in the periodic table [1]. In contrast to other elemental materials, boron has a wide range of bonding options that creates more than 16 bulk polymorphs made up of connected icosahedrons such as α-B_{12}, β-B_{106}, T-B_{192}, and γ-B_{28} [2–5]. A most stable thermodynamic bulk polymorph of boron, β-rhombohedral boron, is an unstable material stabilized by a significant concentration of intrinsic defects that exhibit no ordering even at extremely low temperatures [6]. This is another proof of the uniqueness of boron. This extensive structural variety is also present with two-dimensional (2D) boron sheets. [7]. Piazza et al. first proposed the name of this 2D boron nanosheet as 'borophene' like graphene [8]. Their study provides the first experimental proof of the feasibility of viable unique hexagonal vacancy boron nanostructures. Due to the hexagonal holes, borophene can be subjected to a variety of chemical changes to adjust its electrical and chemical properties. Thus borophene represents a novel family of atom-thick nanomaterial complementary to graphene. In the case of graphene, due to the lack of band gap its usage in digital electronics is limited. Other 2D materials like phosphorene and silicene have restricted their uses in photoelectric and photovoltaic devices due to their instability in the air. Hence, it is extremely necessary to explore a novel 2D semiconductor material that is highly stable in air. Tai et al. carried out first-principles modeling of the electronic band structure which demonstrated the intriguing direct band gap semiconductor properties of the γ-B_{28} monolayer [9].

Borophene has attracted a lot of interest due to its intriguing physical and chemical characteristics, including outstanding mechanical compatibility, excellent carrier mobility, promising optical and electronic properties, extremely high thermal conductivity, and excellent stability [7,9–15]. Borophene has also recently been attracted to the energy, environment, and biomedicine field owing to its outstanding morphological and physicochemical characteristics [7,16–21]. According to theoretical calculations, borophene possesses a variety of

* Corresponding author.
E-mail addresses: arif02me@gmail.com, 19203018@student.duet.ac.bd (A. Rahman), tawabur@eee.kuet.ac.bd (M.T. Rahman), asad@duet.ac.bd (M.A. Chowdhury).
[1] These authors contributed equally.

https://doi.org/10.1016/j.sna.2023.114468
Received 4 April 2023; Received in revised form 1 June 2023; Accepted 2 June 2023
Available online 3 June 2023

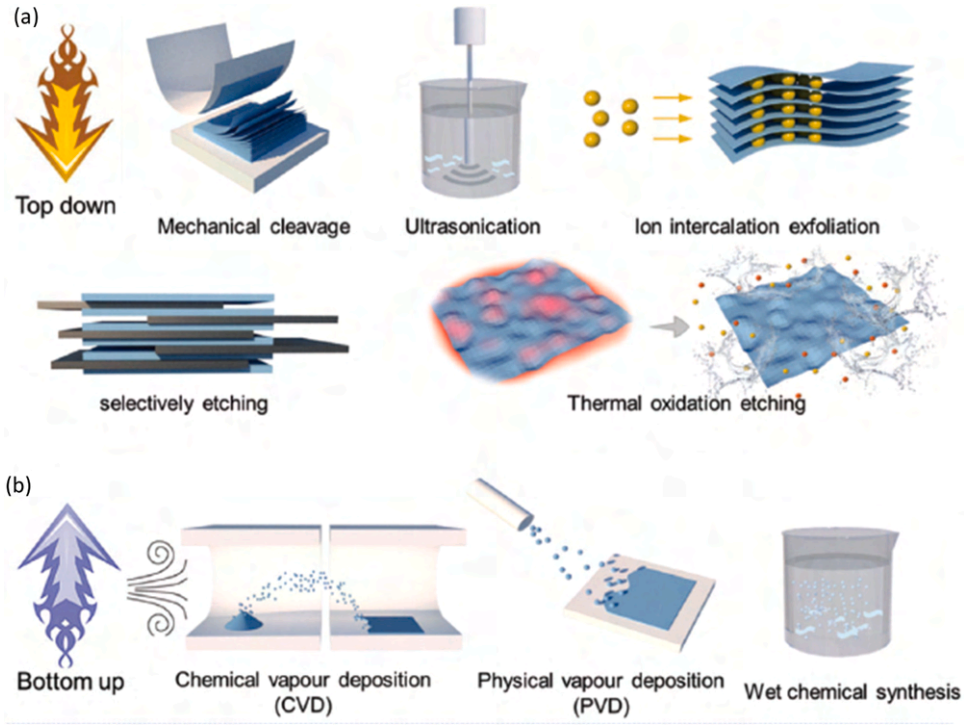

Fig. 1. Synthesis approaches of 2D nanomaterials (a) Top-down approach. (b) Bottom-up approach [34].

low-dimensional allotropes with intriguing characteristics. A few phases of borophene, including 2-Pmmn, β_{12}, χ_3, and graphene-like phases, have been synthesized among the various borophene allotropes. These four different phases of borophene can be synthesized in ultrahigh vacuum (UHV) conditions through chemical vapor deposition (CVD), plasma spray, physical vapor deposition (PVD), liquid phase sonochemical exfoliation, molecular beam epitaxy (MBE), and electron beam evaporation on atomically cleaned substrates [22,23]. According to theoretical predictions, an assortment of borophene structures possesses remarkable Young's moduli [14,15,23]. Generally, the anisotropic Young's modulus triangular structure of borophene is 398 N/m and 170 N/m which is higher than the modulus of graphene in one direction 340 N/m [24]. At first, a successful synthesis of a two-dimensional (2D) boron sheet on silver (Ag) substrates under an ultrahigh-vacuum environment was investigated in 2015 by Mannix et al. [10]. Unlike bulk boron allotropes, borophene exhibits metallic properties that are compatible with forecasts of extremely anisotropic, two-dimensional metal. The four borophene phases (β_{12}, 2-Pmmn, X_3, and honeycomb) that were synthesized throughout the experiments are all metallic [25].

The discovery of synthesis methods and techniques that would enable 2D materials to large production and efficient manipulation is a major problem for the investigation of all 2D materials [26–28]. Sutter et al. investigated the successful large-scale layer-by-layer borophene synthesis up to two single-layer thicknesses through boron segregation on Ru (0001) [29]. The vertical incorporation of borophene by tetraphenyl dibenzo periflanthene (DBP) and angstrom-scale measurement interfacial responses by ultrahigh-vacuum tip-enhanced Raman spectroscopy (UHV-TERS) are examined by Linfei et al. [30]. To direct the experimental growth of borophene, Yakobson et al. have thoroughly explored stable 2D boron sheets [31–33]. However, the experimental implementation of borophene is still in the early stages, therefore additional investigations and theoretical research are required to delve deeper into the material's structures, characteristics, and growth mechanism. In this review, various synthesis methods of borophene have been introduced. Then the structural and morphological characteristics of borophene have been reviewed. Furthermore, the state-of-art theoretical and experimental research on sensing applications of borophene-based devices has been discussed. Finally, the current challenges and future outlook on borophene and borophene-based devices were summarized.

2. Synthesis of borophene

There are two main approaches for synthesizing 2D nanomaterials including top-down and bottom-up. The top-down approach utilizes energy from physical, chemical, and biological sources to split complex structures into smaller pieces. The Top-down approaches include mechanical cleavage, ultrasonication, ion intercalation exfoliation, and different types of etching (Fig. 1a) [34]. The bottom-up approach commences at the atomic scale and utilizes different chemical, physical, or biological interactions for producing the nanoparticles [35]. The bottom-up methods include chemical vapor deposition (CVD), physical vapor deposition (PVD), and wet chemical synthesis (Fig. 1b).

2.1. Top-down approach

Free-standing borophene from boron flakes is produced by Liquid phase sonochemical exfoliation [36]. Lin et al. developed free-standing β_{12} borophene by low-temperature liquid exfoliation (LTLE) method where the temperature range is between -20 to $-25\,^{\circ}C$ [37]. Numerous techniques have been utilized to synthesize borophene, but all of them have some drawbacks such as becoming expensive and difficult for large-scale production. Chowdhury et al. introduce a new temperature-subject electrochemical exfoliation method which is very similar to graphene synthesis. As we know boron is non-conductive material at a low temperature so in this method the heating coil is attached to boron for temperature rises then it can function as a conductive material. The electric heater coil was placed inside the hollow aperture that was retained within the round boron rod in this model. This boron rod was linked to the temperature controller to maintain the desired level of boron temperature. In this method, designated boron acted as the cathode and platinum acted as the anode. Afterward, boron flakes were collected from the solution. Flakes of exfoliated boron were sonicated in acetone for at least two hours to allow them to spread and

Fig. 2. Electrochemical exfoliation of few-layered borophene sheets from bulk boron [52].

form a few atomic layers of borophene. After that, this sonicated solution was then centrifuged at 4000 rpm for 30 min to distinguish the borophene and boron flakes' atomic layers. The layered borophene supernatant solution was then collected and dried [38]. Hou et al. successfully developed ultrastable crystalline hydrogenated borophenes by thermal decomposition of sodium borohydride (NaBH4) [39]. To synthesize borophene without using metal substrates, they designed a three-step heating technic using the thermal decomposition of sodium borohydride under hydrogen as the carrier gas. The developed borophene exhibits remarkable stability in powerful acid and basic solvents and is a unique 2D material with a B1/9 structure. Also, the obtained optical band gap of the borophene agrees well with the first-principles simulations. A borophene-based memory device was ultimately developed to demonstrate a high-performance device application [39].

2.2. Bottom-up approach

The experimental synthesis of borophene is suitable for deposit by Molecular Beam Epitaxy (MBE), Chemical Vapor Deposition (CVD), and Electron Beam Epitaxy (EBE) method on Ag (111) [1,40], Au (111) [41], Cu (111) [42–45], Ir (111) [43,46–48], Al (111) [49], Ru (0001) [29] and quartz [50] substrate. Tai et al. developed atomically thin two-dimensional (2D) γ-boron films on copper Cu foil via CVD using a mixture of boron and boron oxide powder as the boron source and hydrogen gas as the carrier gas [9]. They designed a two-zone CVD furnace for preparing the 2D boron thin films. By using a typical two-zone CVD technique, Y Liu et al. utilized Bis (triphenylphosphine) copper tetrahydroborate ($(Ph_3P)_2$ $Cu(BH_4)$) as a source of boron and successfully synthesized structurally stable and transferrable few-layer β_{12}-borophene on copper foils in a hydrogen-rich atmosphere to stabilize its structure through hydrogenation [51]. Sielicki et al. successfully synthesize the borophene electrochemical exfoliation of boron [52]. This method is carried out by adding bulk boron to a metal mesh, which causes electrical conductivity and creates a platform for the production of borophene. Typically, 0.1 g of bulk boron powder is first prepared on metal mesh (nickel or copper) discs by hydraulic pressing. The disc has a 15 mm diameter and acts as the electrode. There are used two different kinds of electrolytes of LiCl in DMSO and Na_2SO_4 in DI water. The auxiliary electrode is made of platinum wire. An electric current (1 A, 0.5 A, or 0.1 A) is supplied between the cathode and anode throughout the electrochemical exfoliation method. All experiment is carried out for one hour. The supernatant was collected after centrifuging and washing with DI water at 5000 rpm. Fig. 2 displays a graphical illustration of the synthesis of borophene sheets [52].

The discovery of synthesis methods and techniques that would allow for their massive production and efficient processing is a major challenge in the research of all 2D materials [22,53,54]. The same is true for borophene, where investigations are currently mostly limited to a small area of in situ characterizations of samples. Recent advances in methods of synthesis for borophene, substrate source materials, obtained phases, and experiment temperature are summarized in Table 1.

Table 1
Synthesis of borophene by different methods, obtained phases, and operating conditions.

Methods	Substrate	Source material	Phases of borophene	Temperature °C	Ref.
Liquid phase sonochemical exfoliation	Free standing	Boron powder	β_{12}, X_3	-	[36]
Low-temperature exfoliation	Free standing	Boron powder	β_{12}	− 20 to − 25	[37]
Electrochemical exfoliation	Free standing	Boron rod	-	600–1000	[33]
MBE	Ag(111)		Bilayer-α borophene	-	[1]
EBE	Ag(111)	Solid boron rod	$v_{1/5}$, $v_{1/5}$-30°, $v_{1/6}$, and $v_{1/6}$-30°	400–550	[40]
EBE	Au(111)	Boron rod	$v_{1/12}$	550	[41]
MBE	Cu(111)	Boron	β_{12}	326–576	[42]
CVD	Ir(111)	Diborane	χ_6	960	[43]
	Cu(111)	Diborane	χ_3	500	
EBE	Cu(111)	-	-	496	[44]
MBE	Cu(100)		β_{13}	480–550	[45]
Segregation-enhanced epitaxy	Ir(111)	Dorazine $B_3H_6N_3$	χ_6	1200	[46]
CVD	Ir(111)	Borazine	χ_6	850–1100	[47]
EBE	Ir(111)	Boron rod	β_{12} and χ_3	300–600	[48]
MBE	Al(111)	Pure boron	honeycomb	226	[49]
CVD	Quartz	Sodium borohydride ($NaBH_4$)	α2 −'H-borophene	650	[50]
CVD	Ru(0001)	Borazine	-	850–950	[29]
Electrochemical exfoliation	Free-standing	Boron powder	β_{12} or χ_3	-	[52]

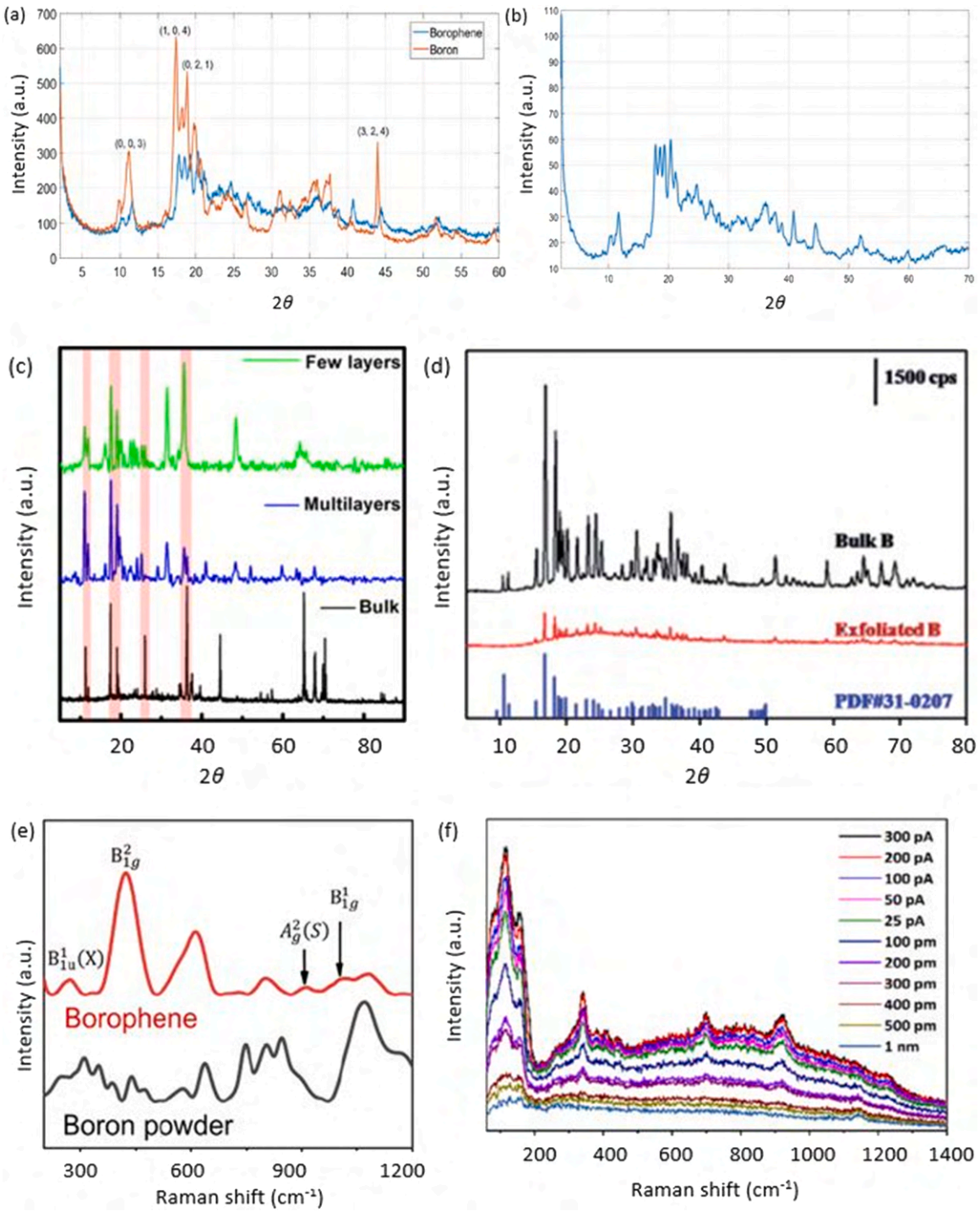

Fig. 3. XRD patterns of the (a) precursor boron microparticles and the prepared borophene [56]. (b) β_{12} borophene [57]. (c) comparative plot of XRD of bulk boron crystal (black), multilayer (blue), and few-layer (green) borophene [59]. (d) XRD patterns of bulk boron and borophene with few layers [58]. (e) Raman spectra of pristine boron powder and 2D borophene sheets [37] (f) Tip-enhanced Raman spectroscopy (TERS) spectrum of α-borophene [64]. (g) Comparison of the TERS spectra of α and β_{12} phases after background subtraction and normalization [64]. Raman spectrum of (h) pure boron powder [61] (i) monolayer β_{12} borophene [61] (j) freestanding borophene [36].

3. Structural and morphological characterization of borophene

X-ray diffraction (XRD) is applied for the primary characterization of material properties such as crystal structure, crystallite size, and strain [55]. Nevin et al. compared the synthesized borophene XRD patterns with boron. From Fig. 3a, it is shown that the boron microparticle and borophene nanoparticle has almost similar peaks [56]. The XRD results showed that there was no phase change when boron microparticles were physically exfoliated to produce borophene and that both boron microparticles and borophene displayed the same crystallinity and β-rhombohedral phase (Fig. 3b). Peaks on the XRD peaks correlated to the boron β-rhombohedra (0001) plane [57]. Chahal et al. has shown that bulk boron crystal displays XRD peaks that resemble the trigonal/rhombohedral (R3m) structure [58]. However, exfoliated sheets

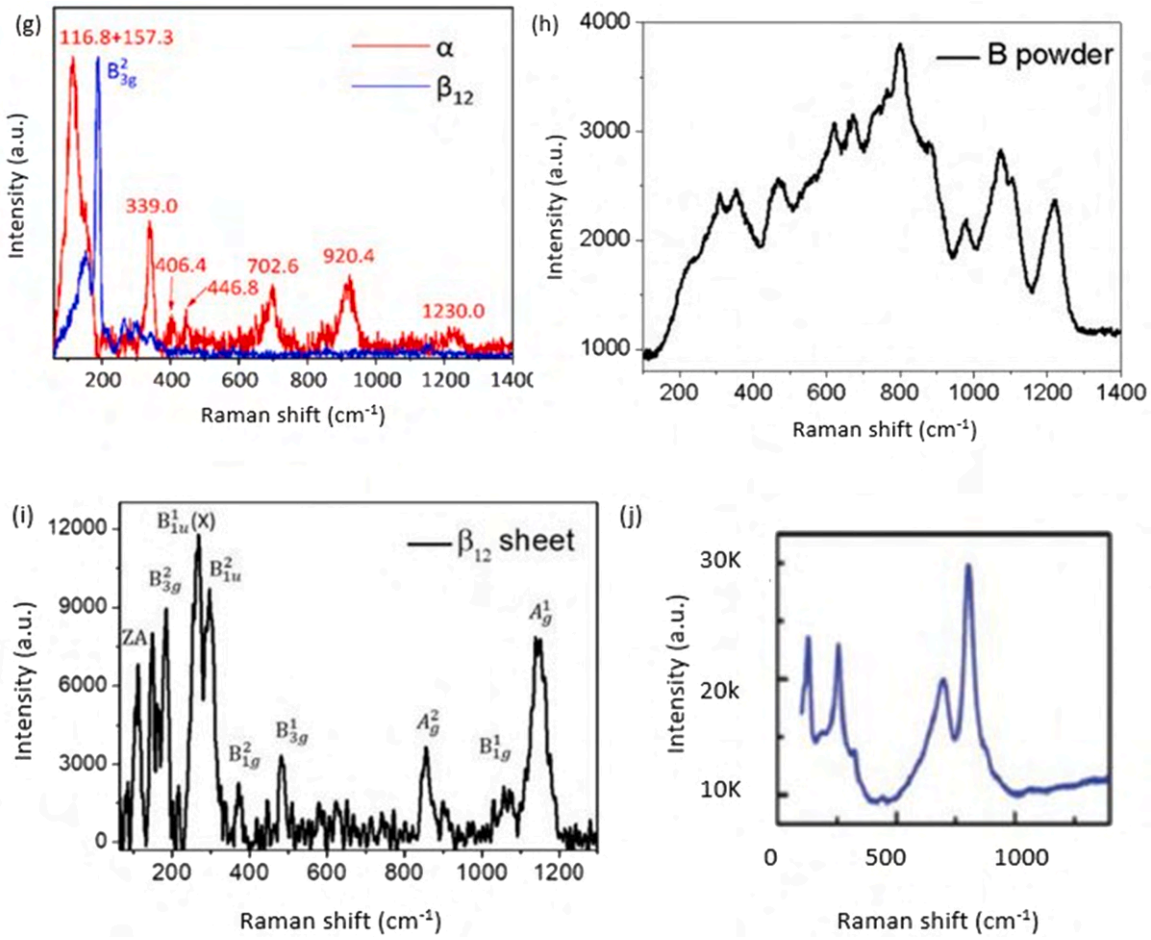

Fig. 3. (*continued*).

exhibited signatures from the parent crystal and new XRD peaks (Fig. 3c), indicating structural changes during exfoliation [59]. Zhang et al. applied XRD to analyze the phase purity and crystalline structure of the exfoliated borophene comparisons the bulk B which are depicted in Fig. 3d. A similar XRD pattern is seen when compared to bulk B, and the majority of the main diffraction peaks can be attributed to the β-rhombohedral boron, indicating that the crystalline structure is almost preserved both before and after exfoliation [58].

Raman spectroscopy is an analytical technic for identifying a material's optical, and vibrational spectroscopic properties, which provides thorough details on molecular composition and molecular structure [60]. The complex structural and chemical characteristics of various boron polymorphs can be characterized by their distinctive Raman spectra, which have been widely utilized to describe bulk boron polymorphs (α, β, and γ-B) [61–63]. Raman spectroscopy was used to distinguish 2D borophene sheets from pure boron powder. In Fig. 3e, the characteristics of the $β_{12}$ phase are readily observed in four Raman peaks of 2D borophene sheets which differ from the pure boron of the β-rhombohedral phase [61]. The strong peak at 268 cm^{-1} is therefore attributed to the out-of-plane bending vibrational modes (B^1_{1u}(X)) of the $β_{12}$ phase, whereas the extra peaks at 423 cm^{-1}, 901 cm^{-1}, and 1017 cm^{-1} are corresponding to the B^2_{1g}, A^2_g (S), and B^1_{1g} modes, respectively, resulting the in-plane straining modes of $β_{12}$ phase [37]. The borophene's vibrational data was obtained using a TERS analysis. The far-field Raman signal is very lower owing to the narrow Raman scattering cross-section for borophene when the STM probe tip is far off from the surface. The Raman signal is dramatically increased when the STM tip is placed near the borophene's surface, showing a substantial increase with the reduction in gap distance. Fig. 3f-g are shown five strong peaks at 116.8 cm^{-1}, 157.3 cm^{-1}, 339.0 cm^{-1}, 702.6 cm^{-1} and 920.4 cm^{-1}, including three poor peaks at 406.4 cm^{-1}, 446.8 cm^{-1} and 1230.0 cm^{-1} [61,64]. According to the Raman spectrum, the pure boron powders which are used for evaporating boron for borophene synthesis found high purity β-rhombohedral phase in Fig. 3h. Raman peaks are exhibited in abundance, particularly at low frequencies. It is noticeably different from the boron powder's Raman spectra, which were used to evaporate boron atoms (Fig. 3i) [61,62]. Ranjan et al. observed sharp Raman peaks for thin sheets of borophene placed over a surface of the gold-coated glass at 130, 258, 697, and 805 cm^{-1} in Fig. 3j [36].

Fourier transform infrared spectroscopy (FTIR) analysis is the method of recognizing organic, inorganic, and polymeric compounds by scanning samples using infrared light [65]. FTIR is a versatile tool for the surface characterization of nanoparticles [66]. The complex structural and chemical properties of Borophene-Quantum Dots with various boron polymorphs and bulk boron were characterized by FTIR spectra. The B-QDs FTIR spectra in Fig. 4a reveal two distinct peaks with centers at 1364 and 3415 cm^{-1} that is attributable to B-O as well as B-OH, respectively. This result suggests that the surfaces of the B-QDs undergo partial boron oxidation [67]. Fig. 4b-c are displayed the FTIR spectra of manufactured borophene as well as the PANI: borophene nanofibrous network. The FTIR study revealed that PANI: Borophene nanofiber network included the distinctive characteristic peaks of the Borophene. The synthesized borophene's FTIR spectrum revealed the sample's typical peaks at 3479 cm^{-1} (O-H), 2929 cm^{-1} (B-B), 2861 cm^{-1} (B-H), 1653 cm^{-1} (C = O), 1496 cm^{-1} (B-H), 1385 cm^{-1} (B-O), 1255 cm^{-1} (B-O), as well as 1091 cm^{-1} (B–O–B vibrations). By the findings, the FTIR spectra of such PANI: Borophene nanofiber identified directly that Borophene was present in the structure and that there were distinct

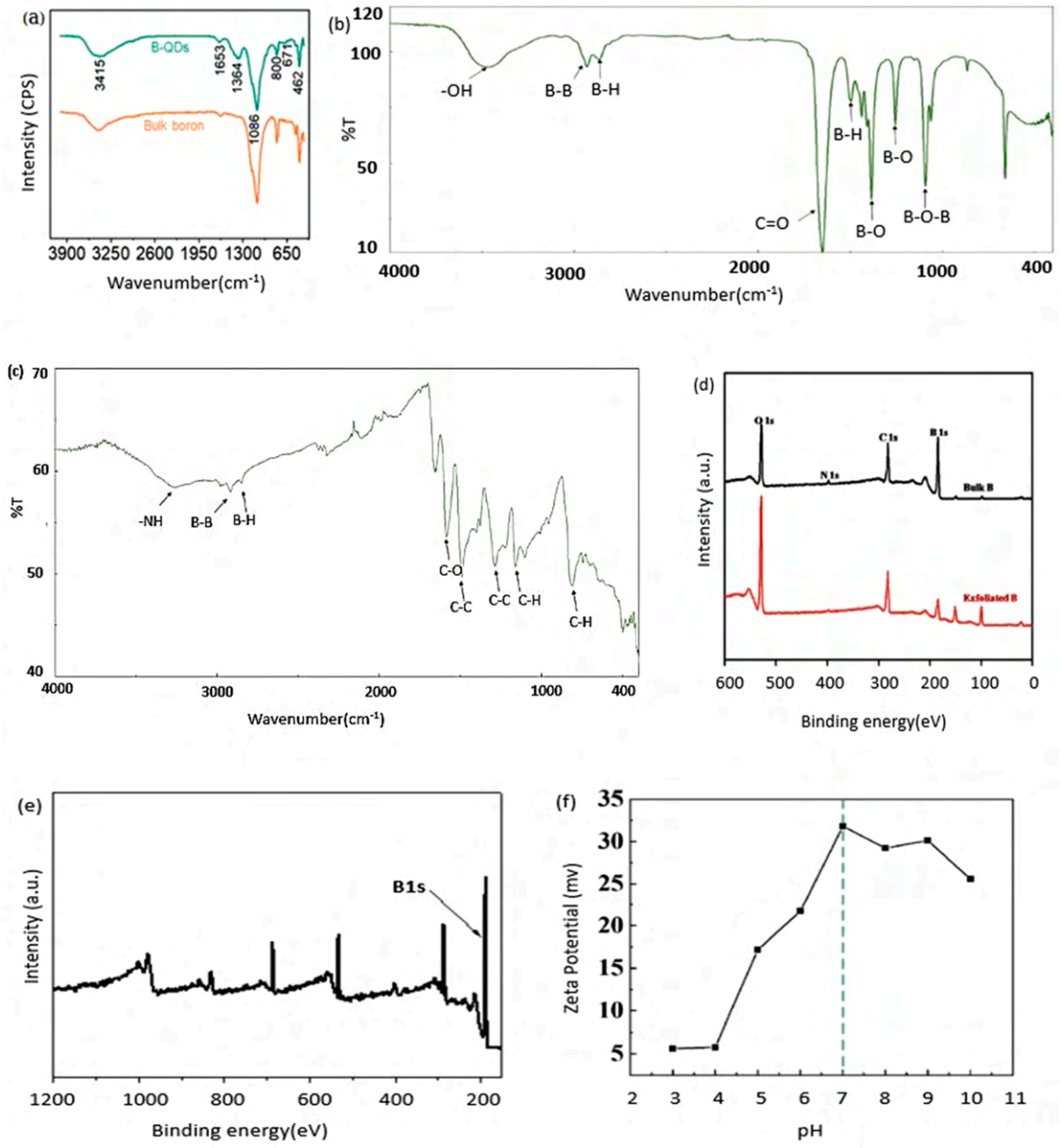

Fig. 4. FTIR spectra of Borophene (a) Quantum Dots and bulk boron [67]. (b) The spectrum of Borophene and (c) PANI: Borophene nanofiber network [68]. (d) XPS spectra of bulk boron and a few layers of borophene [58] and (e) Bulk B and liquid exfoliated Borophene sheets [70]. (f) Borophene glass's zeta potential at various pH levels [50].

bands that were characteristic of Borophene [68].

X-ray photoelectron spectroscopy (XPS) identifies the bonding configurations of metals. XPS is a quantitative method for assessing the elemental structure of a material's surface [69]. XPS was applied to examine the change in the surface's structure and chemical status of borophene layers both before and after exfoliation. Fig. 4d exhibits the bulk B and borophene with a few layers of XPS spectra generated using the probe ultrasound-assisted solvothermal exfoliation method. The main peaks value corresponding to B, C, O, and N have been retained for both samples in the 0–600 eV range of the XPS survey scan spectra of the bulk B and exfoliated borophene, and the B composition doesn't quite change significantly between the two samples, indicating that their surface constituents hardly change both before and after exfoliation [58]. Xiaoyuan et al. exhibit that The XPS spectrum of bulk B as well as liquid exfoliated B sheets comprised only the B ingredient, confirming the remarkable purity of B sheets upon exfoliation (Fig. 4e). Thus, liquid exfoliation of B was detected by X-ray photoelectron spectroscopy (XPS) [70].

The surface charge and physical stability of borophene are evaluated by zeta potential investigation. Zenghui et al. showed how the surface charge of the borophene glass varies on the pH concentrations of various solutions (Fig. 4f). In a neutral solution with a pH of 7, the borophene glass's zeta potential is 31.8 mV which implies that the borophene glass surface is positively charged [50]. Simru et al. reported that the synthesized α-borophene had adequate electrostatic repulsion to attain acceptable physical stability [71]. We find the peak of Zeta potential approximately − 30 mV which is sufficient as Zeta potential is stable $> \pm 30$ mV [72].

Atomic Force Microscopy is a powerful technique for the characterization of nanomaterials both qualitative and quantitative physical properties such as size, surface roughness, morphology, and so forth [73]. Ranjan et al. investigate atomic force microscopy (AFM) that

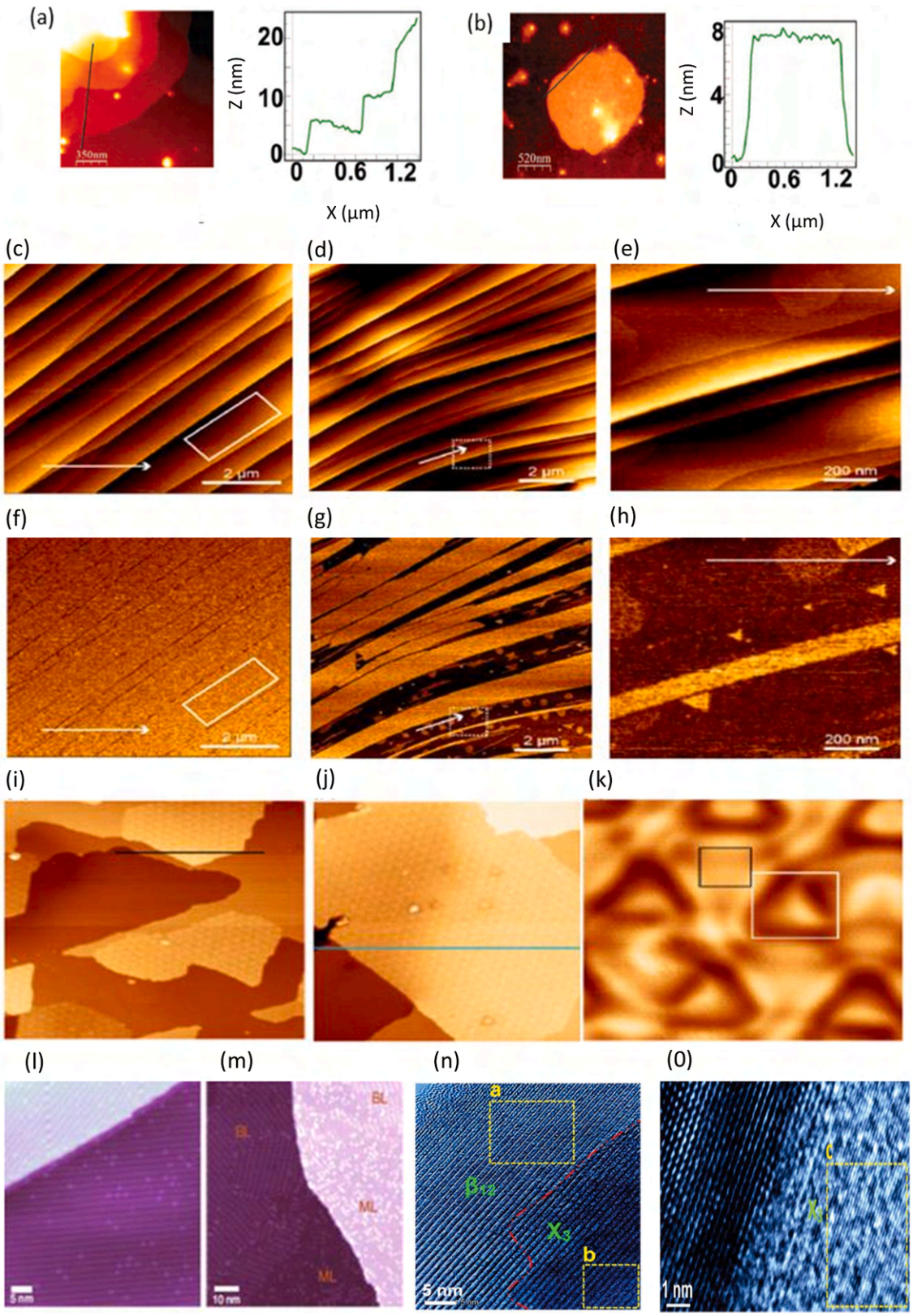

Fig. 5. (a) and (b) AFM images and corresponding thickness profiles for two positions of typical borophene atomic sheets [36]. Borophene scanning on an Ir crystalline using AFM (c) Full Bo coverage area; a white rectangle denotes the area that was checked for roughness. (d) The area is partially covered by borophene sheets and isolated borophene islands. (e) Zoom in on the indicated area (d) by dashed-white square. (f), (g) and (h) the phase scans of (c), (d), and (e) are shown respectively [46]. Single-layer borophene on Al (111) (i) STM picture of borophene (180 nm × 180 nm) islands on the surface of Al (111). (j) A monolayer borophene island is visible in an STM image (150 nm × 150 nm) that covers an Al (111) step. (k) STM picture (15 nm × 15 nm) displaying the triangular corrugation with a large period [49]. (l) Monolayer (ML) borophene onto Cu (111). (m) Borophene coexists in monolayer (ML) and bilayer (BL) [42]. (n) and (o) HRTEM of borophene by the sonochemical method in the acetone solvent having β_{12}, intermediate, and X_3 [36].

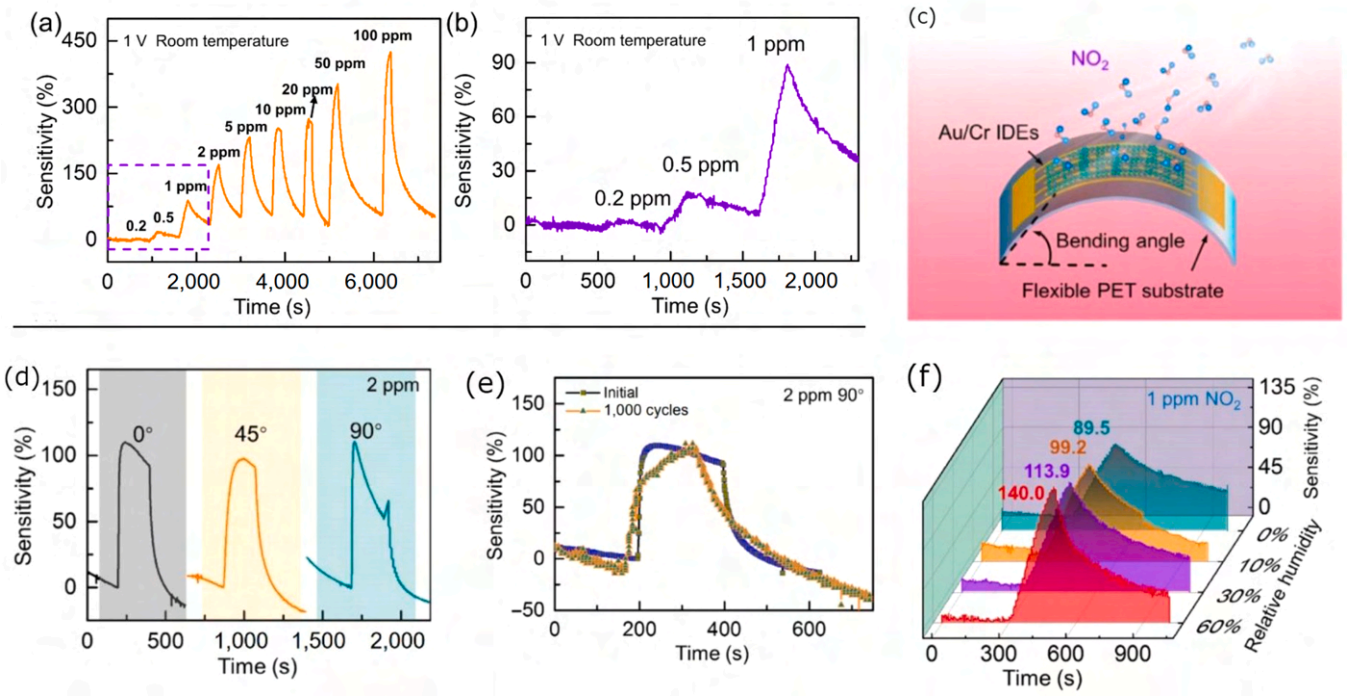

Fig. 6. Borophene sensors' sensing properties at room temperature. (a) Borophene sensing transients at various NO_2 concentrations. (b) The transient response-recovery curve for 0.2, 0.5, and 1 ppm concentrations of NO_2. (c) Schematically illustration of borophene sensor on flexible PET in a bending condition. (d) Real-time response curves for 2 ppm NO_2 at 0°, 45°, and 90° of bending angles respectively. (e) Real-time response curves at 90° bending angles with 1000 cycles (yellow line) and the initial state (blue line). (f) Responses of borophene sensors at room temperature to 1 ppm NO_2 under 0%, 10%, 30%, and 60% RH. Reproduced with permission from [80].

shows borophene sheets are only very few monolayers (1−10) thick as well as vary in thickness. The layered structure of borophene is visualized by AFM. A 2D borophene sheet with a lateral dimension as big as 1.2 m was found in Fig. 5a-b. Although the thickness of the sheets developed can vary, one can extract a monolayer, bilayer, or even multilayer by centrifugation with sufficient speed and timing [36]. Radatović et al. characterized to confirm borophene morphology and stability in ambient conditions using AFM. AFM observation reveals that almost the whole surface is covered by a monolayer of borophene which agrees with the research of Omambac et al. [47]. In Fig. 5c, a large-scale topographic picture shows that borophene crosses numerous terraces. Full coverage and the lack of additional materials on the surface are both confirmed by the corresponding phase image, which is displayed in Fig. 5f. Images 5d and g (topography and phase, respectively) depict partly covered Ir terraces that are frequently decorated by single Bo islands. These characteristics are evident in the AFM phase picture, where different materials provide varied contrasts. Fig. 5e and h depict a zoom-in of the area marked in (Fig. 5d and g) by such a dashed white square (topography and phase, respectively). Particularly in the phase image, individual Bo islands may be distinguished there [46].

Scanning tunneling microscopy (STM) is an approach that has been applied to imaging surfaces at the atomic scale for the surface analysis of nanostructures to use the composition of atoms and molecules in nanoparticles [74,75]. As seen in Fig. 5i-j, monolayer borophene islands are produced when boron is evaporated over a pristine Al (111) substrate at a temperature of roughly 500 K. The surface of the borophene monolayer has distinctive quasi-periodic, triangular corrugations, as seen in high-resolution STM pictures and also the zoom-in scan shown in Fig. 5k [49]. Chen et al. found that borophene was prepared by an electron-beam evaporation method from boron atoms upon the Cu (111) surface at different substrate temperatures (Fig. 5l-m). STM picture exhibits the change in the Cu (111) surface when B coverage increases [42].

Although borophene is expected to exhibit novel mechanical and electrical properties, its large-scale uses are constrained by the need for a substrate and ultrahigh vacuum conditions for borophene deposition, which harms the progress of borophene research. To solve these issues, Pranay et al. demonstrated a facile and large-scale synthesis of free-standing atomic layers of borophene by reducing borophene oxide with a novel liquid-phase exfoliation method [36]. The sonochemical exfoliation technique is utilized to synthesize free-standing borophene with a suitable efficient structure by using boron powder (≈ 20 μm) in different solvents including dimethylformamide, acetone, isopropyl alcohol, water, and ethylene glycol. Acetone performs exceedingly well and results of borophene monolayers compared to other solvents. Besides, borophene showed β_{12}, intermediate, and X_3 phases shown in (Fig. 5n-o).

4. Sensing applications of borophene

Due to the thin layer structures, big surface area, and excellent electronic, physical, and chemical properties, two-dimensional borophene has become a promising material in many applications in the field of sensors, energy storage, optoelectronic devices, etc.[76–78,79,80,26]. Several research groups focused on fabricating borophene-based devices for detecting various gases. For instance, Hou et al. fabricated a borophene-based NO_2 sensor to investigate its gas-sensing ability at room temperature [80]. The resulting sensor revealed excellent sensitivity toward NO_2 in the range of 0.2–100 ppm at room temperature (Fig. 6a-b). The sensor showed an ultrahigh sensitivity of up to 445%, a low detection limit of 200 ppb, and fast response and recovery of 30 s and 200 s, respectively (Fig. 6a). The obtained results are superior to other 2D materials, such as graphene, MoS_2, and phosphorene-based sensors at room temperature [80]. Furthermore, the sensor shows good reproducibility and selectivity to NO_2 gas against various interfering gases. Studying mechanical flexibility and stability for practical applications in the field of flexible electronics is essential. The flexibility of the fabricated borophene sensor on polyethylene terephthalate (PET)

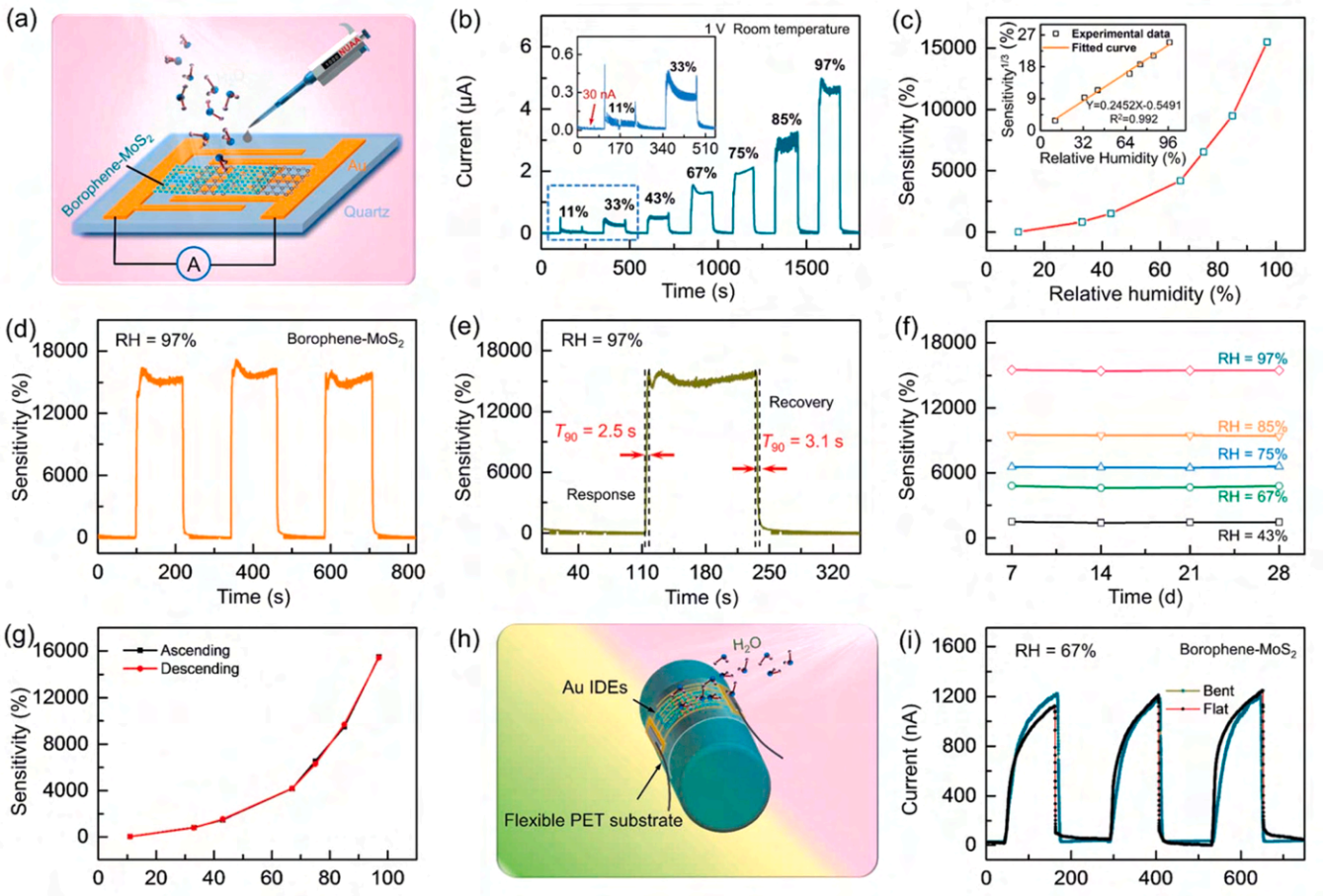

Fig. 7. Fabrication and analysis of borophene–MoS_2 heterostructured humidity sensor. (a) The heterostructured sensor is depicted schematically. (b) Response of the sensor in real-time under switching RH. (c) Sensitivity of the sensor under different RH levels. (d) Sensor cycling stability at 97% RH. (e) Sensor response and recovery curves at 97% RH. (f) The sensor's long-term stability for water vapors is at 43%, 67%, 75%, 85%, and 97% RH. (g) Sensor hysteresis curve at different humidity levels. (h) A bent sensor on a PET substrate is shown schematically. (i) Sensor response curves in flat and bent conditions at 67% RH. Reproduced with permission from [84].

substrate film on the flexible substrate was investigated at three different bending angles including 0°, 45°, and 90° (Fig. 6c). The response curve at 2 ppm NO_2 under the three bending angles is shown in Fig. 6d, where the sensor showed an almost constant sensitivity except for small fluctuation. The possible reason for sensitivity fluctuation can be attributed to the effects of stretching and compression, indicating its high stability under 1000 bending/relaxing cycles in 2 ppm NO_2 gas (Fig. 6e). Thus, the resulting sensor exhibited excellent mechanical flexibility and stability. It is very important to consider the effect of humidity to demonstrate the feasibility of a sensor for its practical applications. The borophene sensor showed an increased sensitivity for 1 ppm of NO_2 with increasing relative humidity (RH from 0% to 60%) (Fig. 6f). This phenomenon can be ascribed to the hole doping effect of H_2O molecules, the large surface area of borophene which causes high adsorption of H_2O, and the production of a large number of hydronium ions (H_3O^+) and H^+, which increase the conductivity of borophene [81, 82].

Stable borophene was successfully synthesized and employed as a promising material in the production of 2D heterostructures. Hou et al. successfully grew large-scale borophene–graphene heterostructure in a hydrogen-rich environment through in situ thermal decompositions of $NaBH_4$ [39]. The prepared borophene–graphene heterostructure has been utilized to construct humidity sensors. The developed sensor showed outstanding performance in detecting humidity at room temperature in the range of 0–85%. The sensitivity of the fabricated borophene-based sensor is nearly 700 times higher than that of pristine graphene at relative humidity (RH) of 85%. Furthermore, the highest sensitivity of 4200% at 85% RH was achieved among all the reported 2D materials-based chemo resistive sensors [83]. Humidity sensors have been also investigated as a promising platform for real-time respiratory monitoring and diagnostic analysis. The theoretical study on borophene–MoS_2 heterostructure showed promise for ultrahigh humidity sensing applications [84]. The fabricated borophene–MoS_2 sensor (Fig. 7a) showed excellent sensitivity, high selectivity, quick response, good stability, and excellent mechanical flexibility. There is a noticeable increase in sensor current and sensitivity with the RH values from 0% to 97% (Fig. 7b and c). The obtained sensitivity at a relative humidity (RH) of 97% is about 15,500%, which is more than 90 or 70 times greater than pristine borophene or MoS_2 (Fig. 7d). To date, this sensitivity is the uppermost among entirely the described chemo resistive sensors based on monolayer materials. Additionally, the resulting sensor showed a faster response and recovery time of 2.5 s and 3.1 s, respectively at 97% RH (Fig. 7e). Compared to other sensors based on MoS_2, graphene, and rGO sheets, the borophene–MoS_2 sensor exhibited alterable sensing properties that will be helpful for the long-life application of the sensor, as depicted in Fig. 7f and g. The selectivity of the sensor was investigated by exposing different interfering gases including ethanol, acetone, toluene, methanol, nitrogen dioxide, and ammonia at room temperature. Excellent selectivity was observed only for water vapor which is important for realizing its practical applications. The borophene–MoS_2 sensor was transferred to a thin and flexible polyethylene terephthalate (PET) substrate attached to a cylindrical rod to realize its flexibility and

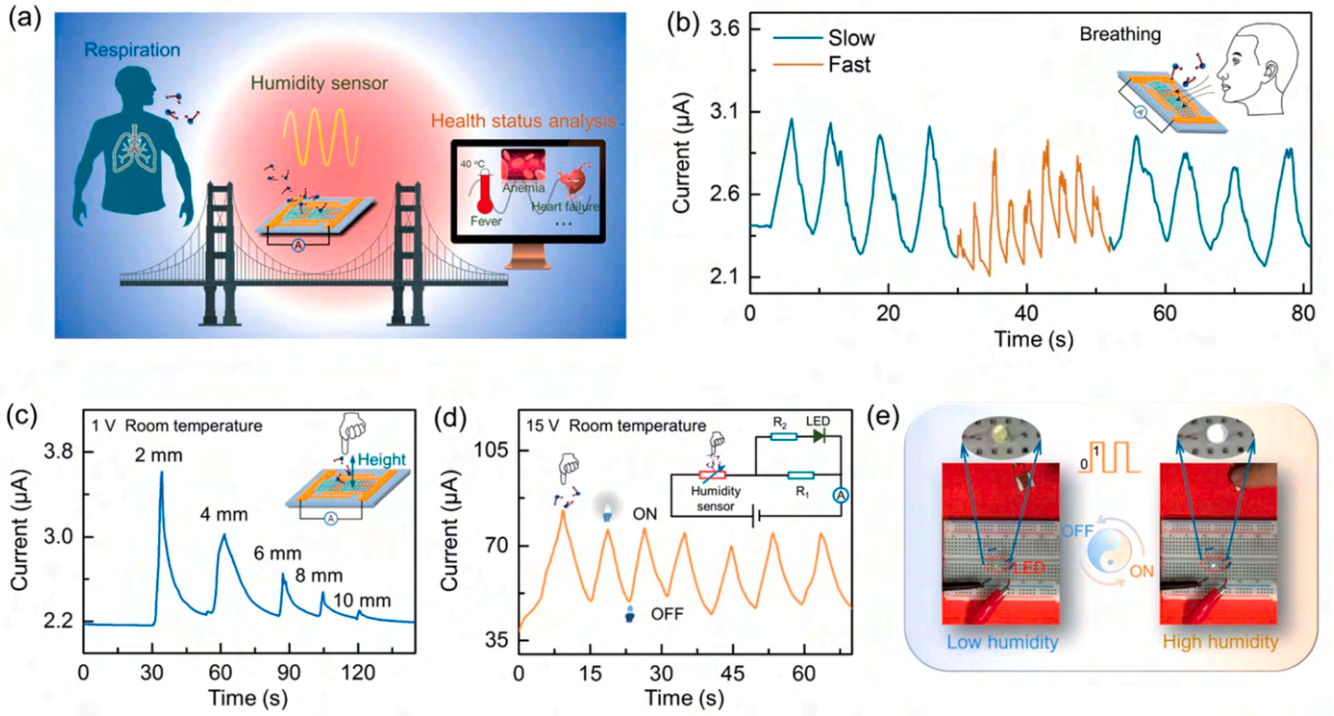

Fig. 8. Applications of the borophene-MoS_2 heterostructured humidity sensor for various purposes. (a) Schematic representation of the human health diagnosis utilizing humidity sensing technology. (b) Response to comparatively slow and fast breathing frequency. (c) Response of the sensor at various fingertip approaching distances. (d) The humidity sensor's response to the current in the non-contact switch sensing system approaches at operation voltages of 15 V both with and without the fingertip. The circuit schematic is inset. (e) Images of a non-contact switch sensing system for the fingertip. The degrees of illumination of a LED light will experience the ON/OFF outcome as a result of the approaching finger.
Reproduced with permission from [84].

stability under high bending strain (Fig. 7h). The sensor maintained almost similar before and after bending because of the greater flexibility of the borophene-MoS_2 heterostructure (Fig. 7i) [84], indicating its potential for flexible and wearable devices used in healthcare [27,28,53,54].

Since the respiration rate controls the human body's health status may harm the length of life revealed by clinical research [85–87]. For instance, extreme breathing rates (>20 breaths per min) may cause fever, pain, anemia and hyperthyroidism, neuropathy, encephalitis, and congestive heart failure may be caused by low breathing rates [85–87]. They employed the developed humidity to form a bridge between the respiration frequency and the diagnosis of diseases (Fig. 8a). Response to slow and fast respiration frequencies was recorded. It was observed that an increase of current happened from about 2.1–3.1 μA at the beginning of exhalation, while it returns to 2 at the beginning of inhalation (Fig. 8b). Thus, the resulting sensor could be used for early diagnosis and prevention without high medical costs. Additionally, surface moisture emitted by fingertips was detected by the humidity sensor for developing a non-contact sensing system. The increased current response was recorded at various distances between the fingertip and the sensor ranging from 2 mm to 10 mm (Fig. 8c-d). When a fingertip approaches a humidity sensor, the sensor's inducing current will increase, leading to an increase in the current of the LED and turning it on (Fig. 8e). Similarly, the current will reduce when the fingertip is maintained away from the sensor, which causes the LED to turn off.

A variety of theoretical simulation approaches including DFT, Non-Equilibrium Green's Function (NEGF), etc., have been studied to explore the gas-sensing capability of borophene materials. Hou et al. demonstrated a strong interaction between borophene and NO_2 molecules (Fig. 9a) [80]. Besides NO_2 molecules act as an acceptor gaining 0.119 e electrons from the borophene, indicating p-type doping of borophene. According to the charge density difference (CCD), the N and O atoms of the NO_2 molecule are surrounded by the golden yellow region (Fig. 9b), indicating the accumulation of lots of electrons that leads to p-type doping of borophene. The band gap of the pristine borophene is found at about 1.05 eV using First-principles calculations (Fig. 9c), whereas the borophene transformed from semiconducting to conducting in nature and consequently the conductivity increased. Because of the adsorption of NO_2 gas (Fig. 9d). Fig. 9e and f show the DOS profile of pristine borophene and the most stable structure after the NO_2 adsorption. Thus, the theoretical computation display that borophene is favorable for sensing NO_2 [80]. DFT calculations showed that the Na-decorated borophene monolayer shows adsorption energy of 1.895 eV and −0.490 eV for CO and CO_2, respectively, which determines borophene as a potential material for capturing and detecting these gases. DFT calculations were further completed to find the adsorption energies of numerous hybrid structures of borophene sensors that showed their long-term stability, selectivity, and electrical conductivity. For instance, the transport properties of borophene/MoS_2 heterostructure were calculated by the NEGF method, showing that the resulting sensor is sensitive toward CO, CO_2, NO, NO_2, and NH_3. Furthermore, the SnO_2 functionalized β_{12}-borophene sheets showed excellent sensitivity toward formaldehyde. A DFT study demonstrated that borophenes exhibited strong chemisorption with C_2H_2 and HCHO molecules, suggesting the usage of borophene as a favorable sensing material for C_2H_2 and HCHO. Fazilaty and coworkers studied the gas ability of X_3-borophene nanoribbon by NEGF and DFT methods. The resulting sensor showed excellent selectivity to H_2S in comparison with NO and H_2O vapor, which can be attributed to the high adsorption energy and strong charge transfer from H_2S to the nanoribbon's edge. For a clear understanding of the chemisorption of SO_2 molecules on the borophene surface, the calculation of adsorption energy and charge transfer was performed for many molecules. It was found that up to seven SO_2 molecules were adsorbed on its surface borophene with a high

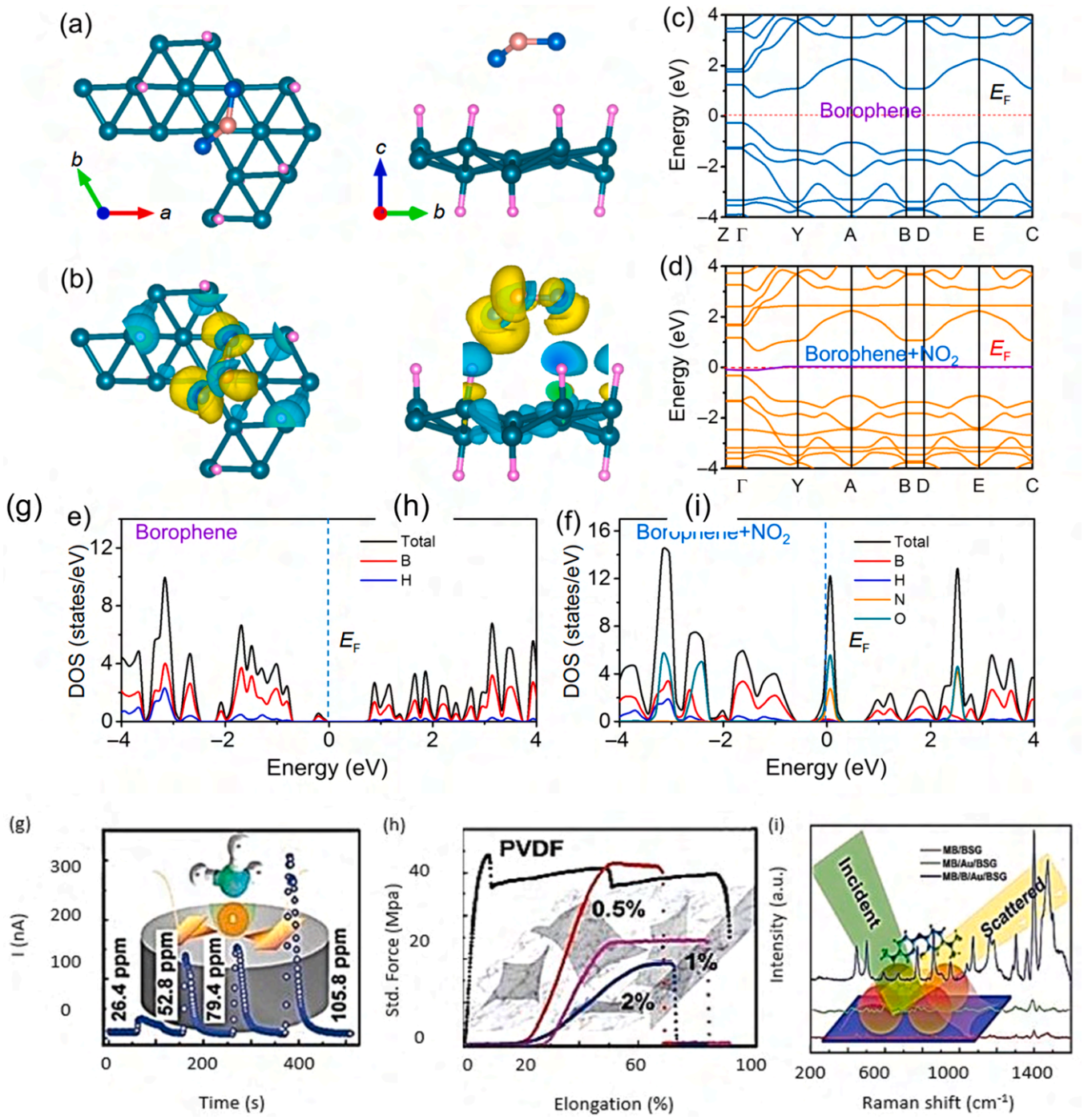

Fig. 9. NO_2 adsorption calculations using DFT on the surface of borophene. (a) Views from the top and sides of the borophene structures with the most stable state. (b) CDD of the configuration. (c) Pristine borophene band structures. (d) Band structures of borophene with adsorption of a single NO_2 molecule. (e) Pristine borophene's DOS. (f) DOS of borophene with NO_2 molecule adsorption. The as-synthesized free-standing borophene sheets (g) ammonia sensing, (h) PVDF sheet with borophene as a nanofiller for strain sensing, (i) molecular sensing by SERS: Raman spectra of methylene blue dye on borosilicate glass, Au/borosilicate glass, and borophene/Au/borosilicate glass.
Reproduced with permission from [80,36].

adsorption energy and charge transfer [94]. The gas sensing characteristics of borophene nanotubes (BNTs) toward trimethyl amine (TMA) and dimethyl amine (DMA) using NEGF and DFT techniques [93]. The peak position in its density of states spectrum shifted, indicating the electron transition between BNT and the target TMA and DMA. The I-V characteristics of the BNT device showed a variation in current with the concentration of DMA and TMA molecules.

A recent report on the B_{36} borophene nanosheet-based device showed significant changes in the electronic properties of borophene (B_{36}) under exposure to HCN due to strong physical and chemisorption. Besides, the β_{12} phases of borophene were successfully synthesized through ultrasonication, which was further functionalized with polyaniline for electrochemical sensing of glucose [95]. Thus, the resulting sensor exhibited an excellent sensitivity to glucose with a low detection limit of 0.5 mM, suggesting borophene is a stable material for the production of 2D heterostructures [83].

Table 2
Sensing applications of borophene-based devices.

Simulation Work					
Species	**Computational method**	**Sensing molecule**	**Mechanism**	**Adsorption energy (eV)**	**Ref.**
Borophene/ MoS_2 heterostructure	DFT and NEGF	CO, CO_2, NO, NO_2, NH_3	Chemisorption and physisorption	-1.15 -0.64 -1.47 - 2.12 -1.52	[88]
β_{12} borophenes	DFT and NEGF	NO, NO_2, and NH_3		-1.13 -1.89 -2.20	[89]
χ3 borophenes	DFT and NEGF	NH_3, NO_2, NO		-1.48 -2.14 -1.93	[89]
β_{12} borophene/ MoS_2	NEGF	CO, NO, NO_2, NH_3	Chemisorption	0.99 0.81 1.63 0.62	[90]
Borophene	DFT	SO_2	Chemisorption	- 3.178	[90]
B_{36} borophene nanosheet	DFT	HCN	Chemisorption	0.19	[91]
β_{12} borophene	DFT	CO, NO, NH3, NO_2, CO_2	Chemisorption	-0.49 -0.38 -0.41 -1.28 -0.19	[92]
Borophene nanotube	NEGF and DFT	DMA and TMA		-1.015 -0.780	[93]
Experimental Work					
Channel material	**Target analyte**	**Sensitivity(%)**	**Detection range**	**Response/recovery**	**Ref.**
Borophene	NO_2	Up to 445%	0.2–100 ppm	30/200 s	[80]
Borophene–graphene	Humidity	4200%	0–85%	10.5/8.3 s	[83]
Borophene-MoS_2	Humidity	15,500%	0–97%	2.5/3.1 s	[84]
$\alpha' - 4$ H- Borophene	Humidity	150%	67–85%	2.3/0.7 s	[83]

Although borophene is expected to exhibit novel mechanical and electrical properties, its large-scale uses are constrained by the necessity for a substrate and ultrahigh vacuum surroundings for borophene deposition, which can harm the progress of borophene research. To solve these issues, Pranay et al. demonstrated a facile and large-scale synthesis of free-standing borophene atomic sheets by a unique liquid-phase exfoliation method and the reduction of borophene oxide [36]. The sonochemical exfoliation technique is utilized to synthesize a free-standing borophene with an energetically advantageous structure. using boron powder ($\approx$ 20 μm) in different solvents including dimethylformamide, acetone, isopropyl alcohol, ethylene glycol, and water. Acetone performs exceedingly well and results in monolayers of borophene compared to other solvents. Inspired by graphene research, it was observed that borophene reacts to light and could be used as a photodetector [96]. It was found that the rise time was 2.4 times faster than the fall time when a two-probe device using borophene as an active material was subjected to a white LED. Borophene is a particularly remarkable surface for ammonia sensing due to its substantially large surface area and, in particular, parallel boron ridges that are spaced apart by $\approx$ 3 Å [82] whereas volatile organic compounds like acetone and ethanol did not react to it. Freestanding borophene's typical reaction time was found to be $\approx$ 7 s for 79.4 ppm (Fig. 9g). In addition to being atomically flat, optically transparent, and having high electrical mobility [97], borophene also exhibits mechanical anisotropy because of atomic ridges that have a higher Young's modulus than graphene along their ridges [98]. PVDF-borophene nanocomposite (0.5 wt% of nanofiller) demonstrates 50% elongation at 40 MPa in contrast to poly (vinylidene difluoride) (PVDF), which shows 8% elongation at 42 MPa, while 1 wt% nano filled PVDF shows 60% elongation at 20 MPa (Fig. 9 h). This demonstrates how borophene strengthens the polymer mechanically. Additionally, when the percentage of nanofiller was raised, a decreased measure of elasticity in the nanocomposite was detected, which may be caused by the clustering of borophene sheets. Surface-enhanced Raman scattering (SERS) using borophene sheets deposited on gold-coated glass has been used to exhibit molecular sensing of methylene blue for 10 ppm (Fig. 9i). Table 2 shows the summary of potential sensing applications for borophene-based devices.

Recently, Wearable pressure sensors have drawn significant attention in the field of robotics, healthcare, artificial intelligence, andhuman–machine interfaces (HMIs) [99,100]. The conventional nanomaterials used for constructing pressure sensors have inevitable drawbacks including poor sensitivity, narrow detection range, difficulties in integrating with semiconductor process, and high-power consumption. To solve these issues, Hou et al. fabricated a novel pressure sensor based on semiconducting hydrogenated borophene using a facile, cost-effective, and versatile approach [101]. It is seen in Fig. 10a that the novel borophene pressure sensor was composed of stacking the borophene and tissue paper on a printed paper substrate with Cr/Au interdigitated electrodes (IDEs). Under various applied static pressures, the resulting current increased dramatically with applying pressure gradually in the range of 0–120 kPa (Fig. 10b). The developed sensor showed highest sensitivity of 2.16 kPa^{-1} when the loading pressure was $<$ 1.2 kPa (Fig. 10c). Subsequently, the sensitivity decreased to about 0.13 kPa^{-1} and 0.07 kPa^{-1} with applied pressures increased from 1.2 to 25 kPa and more than 20 kPa, respectively. This phenomenon can be ascribed to the bulk matrix deformation which became the dominant factor to influence the sensitivity under increasing pressure (Fig. 10b). Besides excellent reproducibility and long-term durability, the borophene-based pressure sensor showed high stability under the pressure of $\sim$ 10 kPa during 1000 dynamic loading and unloading cycles (Fig. 10d). Multifunctional applications of borophene pressure sensor have been demonstrated in Fig. 10 e-i. Fig. 10e shows the real-time wrist pulse signals of a 26-year-old healthy volunteer recorded by the borophene pressure sensor which is promising for human health

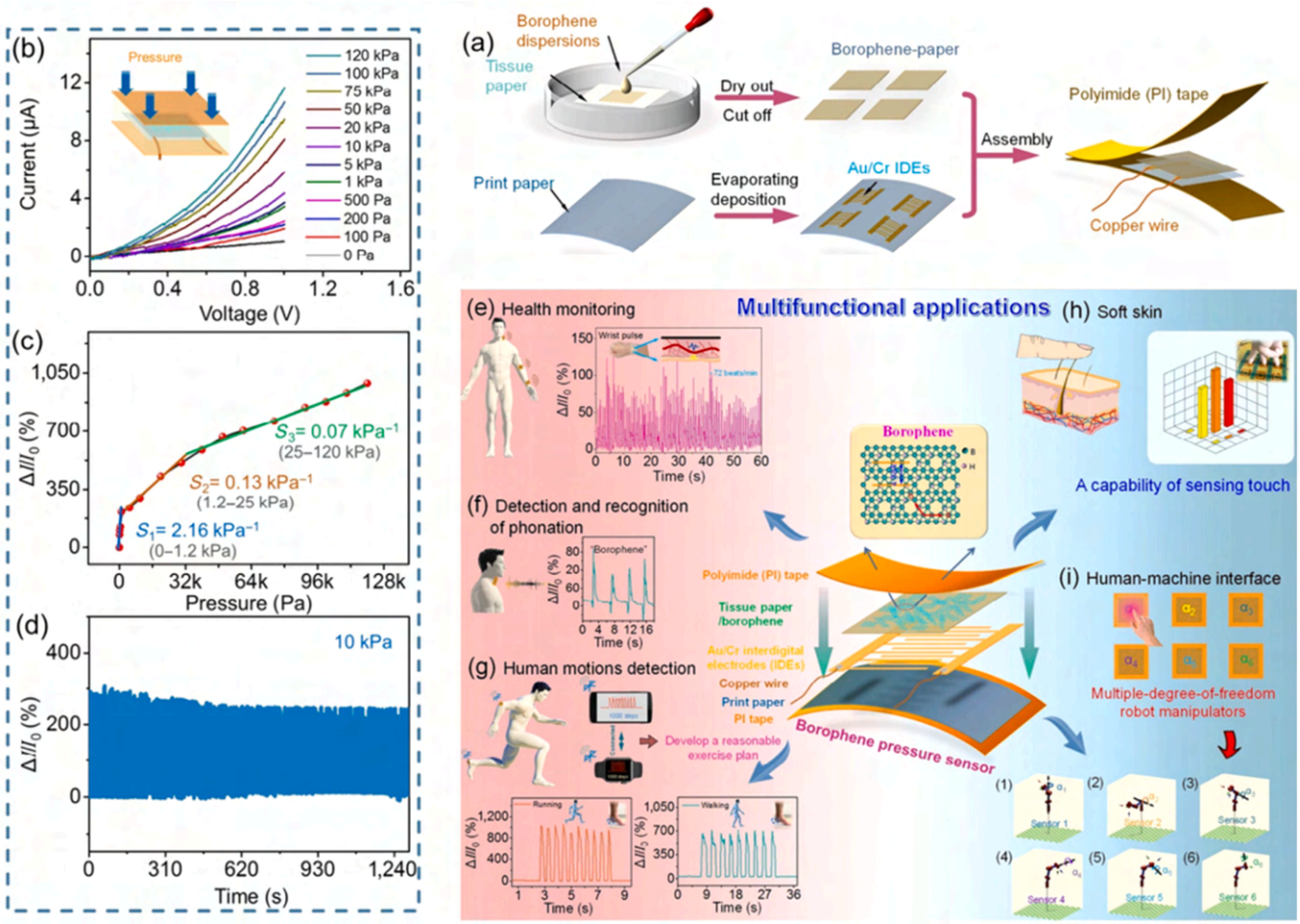

Fig. 10. Fabrication process, electromechanical performances, and multifunctional applications of the borophene pressure sensor. (a) Schematic diagram of fabrication process of the pressure sensor based on borophene and tissue paper. (b) Current–voltage (I–V) characteristics of the fabricated borophene sensor under various applied pressures. (c) Piezoresistive sensitivity of the borophene sensor. (d) Performance of the borophene sensor under repetitive pressure loads of ~ 10 kPa for 1000 cycles. (e)–(i) Multifunctional applications of the borophene pressure sensor: (e) health monitoring, (f) detection and recognition of phonation, (g) human motions detection, (h) soft skin, and (i) human–machine interface [101].

monitoring. It is noteworthy to mention that about 72 peaks were recorded within 1 min, which corresponds to 72 bpm. The skin sensor was attached to the throat of the volunteer and the word "borophene" was pronounced three times, which results the almost same current peaks, confirming its ability for speech recognition. Further, real-time human motion monitoring was also investigated using the skin sensor during running and walking (Fig. 10g). The change of $\Delta I/I_0$ curves generated by running and walking showed good stability and excellent repeatability. Additionally, the sensor also showed an ability to accurately detect and distinguish the different motion rates. Borophene-based electronic skin (e-skin) was realized by developing a sensor array, which results the appearance of three histograms on the monitor with three fingertips touched on the sensor surface (Fig. 10h). The multiple-degree-of-freedom control of the robotic arm is essential to realize the practical applications of the pressure sensor in HMIs. To demonstrate the simulation of robotic arm motions, an array of six borophene sensors, a virtual robotic arm model, and a data acquisition module was constructed (Fig. 10i). Under applied pressure, each sensor array would accurately record the rotation of the robotic arm, which is impressive. Thus, the results pave the way of borophene for pressure sensing and also expand the application of borophene in other sensor devices.

5. Challenges and future prospect of borophene

High-quality synthesis of borophene is a big challenge and also a further challenge is the use of the commercial application and device development for manipulating and transferring Borophene samples to different targeted substrates [14,102]. For the further application of borophene, large-scale synthesis is now also a great challenge. To overcome these challenges Borna et al. demonstrate synthesized single-layer borophene at the macroscopic level and transfer to a Silicon wafer from its initial Ir (111) substrate. But also there remains a limitation to synthesizing top class Borophene samples with remaining thickness uniformly and homogeneous structure and transfer borophene to a suitable substrate with a minimal amount of structural deviation [46]. There are weak adhesion energy between borophene and substrate then silicene and substrate [25].

The borophene's metallic nature and structural instability strictly limit the use of these materials in nanoelectronic and optical devices. Therefore, the stable and semiconducting property for synthesizing borophene is necessary for using them in modern optoelectronics and nanoelectronics applications. For stabilizing borophenes some effective methods can be applied such as hydrogenation, bulking, and substrate assistance [103]. Hydrogenation of borophene is increase the stability of 2-Pmmn and graphene-like borophene phase [80]. A theoretical prediction of borophene is shown that metallic characteristics are transformed into semimetallic characteristics when it is hydrogenated [104].

Due to existing theories of borophene synthesis, the freestanding borophene crystallization is challenging as crystal boron with a 3D structure is not a van der Waals material. Expand bandgap of borophene can be done by strain-engineering like graphene [105,106]. Structural limitations of borophene development restrict the uses in 2D nanomedicine. The high reactivity of boron with metals such as CoB_8 and RuB-, IrB_9-, FeB_8, and FeB_9- limits its biomedical applications which have been proven harmful to humans. Synthesis of borophene by liquid phase chemical exfoliation also restricts biomedical application as this process uses toxic precursors [107]. The usage of toxic agents in the synthesis process must also be taken into account. Liquid-phase electrochemical exfoliation approaches would be the first option for synthesizing borophene in larger quantities. But the use of hydrochloric acid for etching and toxic precursors limits borophene in biomedical applications. Though electron beam evaporation may stop the usage of precursors, it is expensive and only appropriate for laboratories [11]. The applications of borophene for sensing devices, photodetectors, and energy storage are yet largely unexplored. Thus, there are still a lot of intriguing features and device applications of borophene to be investigated.

6. Conclusions

This review summarizes the recent advancements in borophene synthesis, characterization, applications, and challenges. A variety of synthesis techniques for preparing borophene including CVD, MBE, EBE, liquid phase exfoliation, and electrochemical exfoliation are briefly discussed. Since boron is non-conductive at low temperatures, so Chowdhury et al. introduced a novel temperature-assisted electrochemical method for the preparation of conductive boron [38]. In another report, electric current was applied to metal mesh mixed with boron powder for preparing conductive borophene [47]. The literature associated with the borophene synthesis by MBE, CVD, and free-standing exfoliation exhibit structural instability limitations and the borophene Field's metallic nature [104]. Due to these constraints, the applications of the prepared borophene have been limited to use in nanoelectronic and optical devices. The synthesis of borophene has been carried out on different metal substrates including Ag (111), Ir (111), Cu (111), Au (111), Ir (111), quartz, Al (111), Ru (0001), Ir (111), and Cu (100) by using liquid phase sonochemical exfoliation, MBE, EBE, and CVD [36–52]. Different phases of borophene including β_{12}, χ_3, χ_6, and honeycomb are successfully synthesized on metal substrates. Atomic scale characterizations of 2D borophene have been explained thoroughly in this review. For further uses of borophene, large-scale production of quality-controlled borophene remains a significant challenge. Although CVD and MBE provide high-quality and defect-free borophene, these methods suffer from high cost and small-scale production. To develop structurally stable borophene, efforts have been made such as hydrogenation. Also, the metallic nature of borophene limits its application to a semiconductor device. So, doping should be another option for preparing semiconducting borophene for its application in nanoelectronics and optoelectronics devices. Borophene showed its potential for various applications in the field of toxic gas sensing including NO_2, NH_3, NO, SO_2, etc., along with humidity sensing, and photodetectors. The incorporation of MoS_2 into borophene made it promising for ultrahigh humidity sensing applications. Moreover, borophene-based devices showed excellent mechanical flexibility which is potential for flexible and wearable devices used in healthcare. Although some advances have been made recently in the field of borophene research, the experimental comprehension of borophene is quiet in its early stages. More experimental and theoretical efforts are still required to discover the structures and properties and the growth mechanism of borophene.

Declaration of Competing Interest

The authors declare no conflict of interest.

Data availability

Data will be made available on request.

References

[1] X. Liu, Q. Li, Q. Ruan, M.S. Rahn, B.I. Yakobson, M.C. Hersam, Borophene synthesis beyond the single-atomic-layer limit, Nat. Mater. vol. 21 (1) (2022) 35–40, https://doi.org/10.1038/S41563-021-01084-2.

[2] X. Liu, Q. Li, Q. Ruan, M.S. Rahn, B.I. Yakobson, M.C. Hersam, Borophene synthesis beyond the single-atomic-layer limit, Nat. Mater. vol. 21 (1) (2022) 35–40, https://doi.org/10.1038/s41563-021-01084-2.

[3] H.J. Zhai, B. Kiran, J. Li, L.S. Wang, Hydrocarbon analogues of boron clusters planarity, aromaticity and antiaromaticity, Nat. Mater. vol. 2 (12) (2003) 827–833, https://doi.org/10.1038/nmat1012.

[4] H.J. Zhai, A.N. Alexandrova, K.A. Birch, A.I. Boldyrev, L.S. Wang, Hepta- and octacoordinate boron in molecular wheels of eight- and nine-atom boron clusters: observation and confirmation, Angew. Chem. Int. Ed. vol. 42 (48) (2003) 6004–6008, https://doi.org/10.1002/ANIE.200351874.

[5] T. Ogitsu, E. Schwegler, G. Galli, β-Rhombohedral boron: at the crossroads of the chemistry of boron and the physics of frustration, Chem. Rev. vol. 113 (5) (2013) 3425–3449, https://doi.org/10.1021/CR300356T/SUPPL_FILE/CR300356T_SI_002.ZIP.

[6] T. Ogitsu, F. Gygi, J. Reed, Y. Motome, E. Schwegler, G. Galli, Imperfect crystal and unusual semiconductor: Boron, a frustrated element, J. Am. Chem. Soc. vol. 131 (5) (2009) 1903–1909, https://doi.org/10.1021/JA807622W/SUPPL_FILE/JA807622W_SI_001.PDF.

[7] A.J. Mannix, Z. Zhang, N.P. Guisinger, B.I. Yakobson, M.C. Hersam, Borophene as a prototype for synthetic 2D materials development, Nat. Nanotechnol. vol. 13 (6) (2018) 444–450, https://doi.org/10.1038/S41565-018-0157-4.

[8] Z.A. Piazza, H.S. Hu, W.L. Li, Y.F. Zhao, J. Li, L.S. Wang, Planar hexagonal B36 as a potential basis for extended single-atom layer boron sheets, Nat. Commun. vol. 5 (1) (2014) 1–6, https://doi.org/10.1038/ncomms4113.

[9] G. Tai, et al., Synthesis of atomically thin boron films on copper foils, Angew. Chem. Int. Ed. vol. 54 (51) (2015) 15473–15477, https://doi.org/10.1002/ANIE.201509285.

[10] A.J. Mannix, et al., Synthesis of borophenes: anisotropic, two-dimensional boron polymorphs, Science vol. 350 (6267) (2015) 1513–1516, https://doi.org/10.1126/SCIENCE.AAD1080.

[11] B. Feng, et al., Experimental realization of two-dimensional boron sheets, Nat. Chem. vol. 8 (6) (2016) 563–568, https://doi.org/10.1038/NCHEM.2491.

[12] X. Liu, M.C. Hersam, 2D materials for quantum information science, Nat. Rev. Mater. vol. 4 (10) (2019) 669–684, https://doi.org/10.1038/S41578-019-0136-X.

[13] Z. Wu, G. Tai, W. Shao, R. Wang, C. Hou, Experimental realization of quasicubic boron sheets, Nanoscale vol. 12 (6) (2020) 3787–3794, https://doi.org/10.1039/C9NR08967E.

[14] Z. Zhang, E.S. Penev, B.I. Yakobson, Two-dimensional boron: structures, properties and applications, Chem. Soc. Rev. vol. 46 (22) (2017) 6746–6763, https://doi.org/10.1039/C7CS00261K.

[15] Z. Wu, Y. Yin, C. Hou, G. Tai, Borophene reinforcing copper matrix composites: preparation and mechanical properties, J. Alloy. Compd. vol. 930 (2023), 167370, https://doi.org/10.1016/J.JALLCOM.2022.167370.

[16] H. Li, et al., Scalable production of few-layer boron sheets by liquid-phase exfoliation and their superior supercapacitive performance, ACS Nano vol. 12 (2) (2018) 1262–1272, https://doi.org/10.1021/ACSNANO.7B07444.

[17] A. Molle, J. Goldberger, M. Houssa, Y. Xu, S.C. Zhang, D. Akinwande, Buckled two-dimensional Xene sheets, Nat. Mater. vol. 16 (2) (2017) 163–169, https://doi.org/10.1038/nmat4802.

[18] X. Sun, et al., Two-dimensional boron crystals: structural stability, tunable properties, fabrications and applications, Adv. Funct. Mater. vol. 27 (19) (2017) 1603300, https://doi.org/10.1002/ADFM.201603300.

[19] X. Zhang, et al., Boron nanosheet: an elemental two-dimensional (2D) material for ambient electrocatalytic N2-to-NH3 fixation in neutral media, ACS Catal. vol. 9 (5) (2019) 4609–4615, https://doi.org/10.1021/ACSCATAL.8B05134/SUPPL_FILE/CS8B05134_SI_001.PDF.

[20] S.Y. Xie, Y. Wang, X. Bin Li, Flat boron: a new cousin of graphene, Adv. Mater. vol. 31 (36) (2019) 1900392, https://doi.org/10.1002/ADMA.201900392.

[21] M. Han, et al., Protein corona and immune responses of borophene: a comparison of nanosheet-plasma interface with graphene and phosphorene, ACS Appl. Bio Mater. vol. 3 (7) (2020) 4220–4229, https://doi.org/10.1021/ACSABM.0C00306/SUPPL_FILE/MT0C00306_SI_001.PDF.

[22] A. Rahman, M.A. Chowdhury, N. Hossain, M. Rana, M.J. Alam, A review of the tribological behavior of electrodeposited cobalt (Co) based composite coatings, Compos. Part C Open Access vol. 9 (2022), 100307, https://doi.org/10.1016/J.JCOMC.2022.100307.

[23] Y.V. Kaneti, D.P. Benu, X. Xu, B. Yuliarto, Y. Yamauchi, D. Golberg, Borophene: two-dimensional boron monolayer: synthesis, properties, and potential applications, Chem. Rev. vol. 122 (1) (2022) 1000–1051, https://doi.org/10.1021/ACS.CHEMREV.1C00233/ASSET/IMAGES/MEDIUM/CR1C00233_0042.GIF.

[24] Z. Zhang, Y. Yang, E.S. Penev, B.I. Yakobson, Elasticity, Flexibility, and Ideal Strength of Borophenes, DOI: 10.1002/adfm.201605059.

[25] Z.Q. Wang, T.Y. Lü, H.Q. Wang, Y.P. Feng, J.C. Zheng, Review of borophene and its potential applications, Front. Phys. vol. 14 (3) (2019) 33403, doi: 10.1007/S11467-019-0884-5.

[26] M.T. Rahman, R. Kumar, M. Kumar, Q. Qiao, Two-dimensional transition metal dichalcogenides and their composites for lab-based sensing applications: recent progress and future outlook, Sens. Actuators A Phys. vol. 318 (2021), 112517.

[27] M.T. Rahman, et al., Graphene oxide–silver nanowire nanocomposites for enhanced sensing of Hg2, ACS Appl. Nano Mater. vol. 2 (8) (2019) 4842–4851.

[28] M.T. Rahman, et al., Metallic 1T phase tungsten disulfide microflowers for trace level detection of Hg2+ ions, Adv. Sustain. Syst. vol. 4 (9) (2020) 2000068.

[29] P. Sutter, E. Sutter, Large-scale layer-by-layer synthesis of borophene on Ru (0001), Chem. Mater. vol. 33 (22) (2021) 8838–8843, https://doi.org/10.1021/ACS.CHEMMATER.1C03061/SUPPL_FILE/CM1C03061_SI_003.AVI.

[30] L. Li, et al., Angstrom-scale spectroscopic visualization of interfacial interactions in an organic/borophene vertical heterostructure, J. Am. Chem. Soc. vol. 143 (38) (2021) 15624–15634, https://doi.org/10.1021/JACS.1C04380/SUPPL_FILE/JA1C04380_SI_001.PDF.

[31] I. Boustani, Systematic ab initio investigation of bare boron clusters: mDetermination of the geometry and electronic structures of B_n (n=2–14), Phys. Rev. B, 55(24), 1997, p. 16426. DOI: 10.1103/PhysRevB.55.16426.

[32] H. Tang, S. Ismail-Beigi, Novel precursors for boron nanotubes: the competition of two-center and three-center bonding in boron sheets, Phys. Rev. Lett. vol. 99 (11) (2007), https://doi.org/10.1103/PHYSREVLETT.99.115501.

[33] Y. Liu, E.S. Penev, B.I. Yakobson, Probing the synthesis of two-dimensional boron by first-principles computations, Angew. Chem. Int. Ed. vol. 52 (11) (2013) 3156–3159, https://doi.org/10.1002/ANIE.201207972.

[34] M. Ou, et al., The emergence and evolution of borophene, Adv. Sci. vol. 8 (12) (2021) 2001801, https://doi.org/10.1002/ADVS.202001801.

[35] A. Rahman, M.A. Chowdhury, N. Hossain, Green synthesis of hybrid nanoparticles for biomedical applications: A review, Appl. Surf. Sci. Adv. vol. 11 (2022), 100296, https://doi.org/10.1016/J.APSADV.2022.100296.

[36] P. Ranjan, et al., Freestanding borophene and its hybrids, Adv. Mater. vol. 31 (27) (2019) 1900353, https://doi.org/10.1002/ADMA.201900353.

[37] H. Lin, et al., Scalable production of freestanding few-layer β12-borophene single crystalline sheets as efficient electrocatalysts for lithium-sulfur batteries, ACS Nano vol. 15 (11) (2021) 17327–17336, https://doi.org/10.1021/ACSNANO.1C04961/SUPPL_FILE/NN1C04961_SI_001.PDF.

[38] M.A. Chowdhury, M.M.K. Uddin, M.B.A. Shuvho, M. Rana, N. Hossain, A novel temperature dependent method for borophene synthesis, Appl. Surf. Sci. Adv. vol. 11 (2022), 100308, https://doi.org/10.1016/J.APSADV.2022.100308.

[39] C. Hou, G. Tai, J. Hao, L. Sheng, B. Liu, Z. Wu, Ultrastable crystalline semiconducting hydrogenated borophene, Angew. Chem. Int. Ed. vol. 59 (27) (2020) 10819–10825, https://doi.org/10.1002/ANIE.202001045.

[40] Q. Li, et al., Synthesis of borophane polymorphs through hydrogenation of borophene, Science vol. 371 (6534) (2021) 1143–1148, https://doi.org/10.1126/SCIENCE.ABG1874.

[41] B. Kiraly, et al., Borophene synthesis on Au(111), ACS Nano vol. 13 (4) (2019) 3816–3822, https://doi.org/10.1021/ACSNANO.8B09339/SUPPL_FILE/NN8B09339_SI_001.PDF.

[42] C. Chen, et al., Synthesis of bilayer borophene, Nat. Chem. vol. 14 (1) (2021) 25–31, https://doi.org/10.1038/s41557-021-00813-z.

[43] M.G. Cuxart, et al., Borophenes made easy, Sci. Adv. vol. 7 (45) (2021), https://doi.org/10.1126/SCIADV.ABK1490.

[44] R. Wu, et al., Large-area single-crystal sheets of borophene on Cu(111) surfaces, Nat. Nanotechnol. vol. 14 (1) (2018) 44–49, https://doi.org/10.1038/S41565-018-0317-6.

[45] R. Wu, et al., Micrometre-scale single-crystalline borophene on a square-lattice Cu(100) surface, Nat. Chem. vol. 14 (4) (2022) 377–383, https://doi.org/10.1038/S41557-021-00879-9.

[46] B. Radatović, et al., Macroscopic single-phase monolayer borophene on arbitrary substrates, ACS Appl. Mater. Interfaces (2022), https://doi.org/10.1021/ACSAMI.2C03678/SUPPL_FILE/AM2C03678_SI_001.PDF.

[47] K.M. Omambac, et al., Segregation-enhanced epitaxy of borophene on Ir(111) by thermal decomposition of borazine, ACS Nano vol. 15 (4) (2021) 7421–7429, https://doi.org/10.1021/ACSNANO.1C00819/SUPPL_FILE/NN1C00819_SI_001.PDF.

[48] N.A. Vinogradov, A. Lyalin, T. Taketsugu, A.S. Vinogradov, A. Preobrajenski, Single-phase borophene on Ir(111): formation, structure, and decoupling from the support, ACS Nano vol. 13 (12) (2019) 14511–14518, https://doi.org/10.1021/ACSNANO.9B08296.

[49] W. Li, et al., Experimental realization of honeycomb borophene, Sci. Bull. (2018), https://doi.org/10.1016/j.scib.2018.02.006.

[50] Z. Wu, G. Tai, R. Liu, W. Shao, C. Hou, X. Liang, Synthesis of borophene on quartz towards hydroelectric generators, J. Mater. Chem. A vol. 10 (15) (2022) 8218–8226, https://doi.org/10.1039/D1TA10855G.

[51] Y. Liu, G. Tai, C. Hou, Z. Wu, X. Liang, Chemical vapor deposition growth of few-layer β12-borophane on copper foils toward broadband photodetection, ACS Appl. Mater. Interfaces (2023), https://doi.org/10.1021/ACSAMI.2C23234/SUPPL_FILE/AM2C23234_SI_001.PDF.

[52] K. Sielicki, K. Maślana, X. Chen, E. Mijowska, Bottom up approach of metal assisted electrochemical exfoliation of boron towards borophene, Sci. Rep. vol. 12 (1) (2022) 1–7, https://doi.org/10.1038/s41598-022-20130-w.

[53] M.F. Kabir, M.T. Rahman, A. Gurung, Q. Qiao, Electrochemical phosphate sensors using silver nanowires treated screen printed electrodes, IEEE Sens. J. vol. 18 (9) (2018) 3480–3485.

[54] A. Sobhan, K. Muthukumarappan, L. Wei, Q. Qiao, M.T. Rahman, N. Ghimire, Development and characterization of a novel activated biochar-based polymer composite for biosensors, Int. J. Polym. Anal. Charact. vol. 26 (6) (2021) 544–560.

[55] N. Raval, R. Maheshwari, D. Kalyane, S.R. Youngren-Ortiz, M.B. Chougule, R. K. Tekade, Importance of physicochemical characterization of nanoparticles in pharmaceutical product development, Basic Fundam. Drug Deliv. (2018) 369–400, https://doi.org/10.1016/B978-0-12-817909-3.00010-8.

[56] N. Taşaltın, C. Taşaltın, S. Güngör, S. Karakuş, İ. Gürol, M. Teker, Volatile organic compound detection performance of Borophene and PANI:β Borophene nanocomposite-based sensors, J. Mater. Sci. Mater. Electron. (2022), https://doi.org/10.1007/S10854-022-09109-5.

[57] S. Güngör, C. Taşaltın, İ. Gürol, G. Baytemir, S. Karakuş, N. Taşaltın, Copper phthalocyanine-borophene nanocomposite-based non-enzymatic electrochemical urea biosensor, Appl. Phys. A Mater. Sci. Process. vol. 128 (1) (2022) 1–8, https://doi.org/10.1007/S00339-021-05228-8/METRICS.

[58] F. Zhang, et al., Few-layer and large flake size borophene: preparation with solvothermal-assisted liquid phase exfoliation, RSC Adv. vol. 10 (46) (2020) 27532–27537, https://doi.org/10.1039/D0RA03492D.

[59] S. Chahal, et al., Borophene via micromechanical exfoliation, Adv. Mater. vol. 33 (34) (2021) 2102039, https://doi.org/10.1002/ADMA.202102039.

[60] R. Wolthuis, et al.. Raman Spectroscopic Methods for in Vitro and in Vivo Tissue Characterization, Chapter Thirty-two Vol. 11, 1999, p. 216, ill.

[61] S. Sheng, et al., Raman spectroscopy of two-dimensional borophene sheets, ACS Nano vol. 13 (4) (2019) 4133–4139, https://doi.org/10.1021/acsnano.8b08909.

[62] H. Werheit, et al., Raman effect in icosahedral boron-rich solids, Sci. Technol. Adv. Mater. vol. 11 (2) (2010), https://doi.org/10.1088/1468-6996/11/2/023001.

[63] G. Parakhonskiy, V. Vtech, N. Dubrovinskaia, R. Caracas, L. Dubrovinsky, Raman spectroscopy investigation of alpha boron at elevated pressures and temperatures, Solid State Commun. vol. 154 (1) (2013) 34–39, https://doi.org/10.1016/J.SSC.2012.10.026.

[64] P. Zhang, et al., Vibrational property of α-borophene determined by tip-enhanced raman spectroscopy, Molecules vol. 27 (3) (2022) 834, https://doi.org/10.3390/MOLECULES27030834.

[65] D. Titus, E. James Jebaseelan Samuel, S.M. Roopan, Nanoparticle characterization techniques, Green Synth. Charact. Appl. Nanopart. (2019) 303–319, https://doi.org/10.1016/B978-0-08-102579-6.00012-5.

[66] K. Torres-Rivero, J. Bastos-Arrieta, N. Fiol, A. Florido, Metal and metal oxide nanoparticles: an integrated perspective of the green synthesis methods by natural products and waste valorization: applications and challenges, Compr. Anal. Chem. vol. 94 (2021) 433–469, https://doi.org/10.1016/BS.COAC.2020.12.001.

[67] H. Wang, et al., Crystalline borophene quantum dots and their derivative boron nanospheres, Mater. Adv. vol. 2 (10) (2021) 3269–3273, https://doi.org/10.1039/D1MA00124H.

[68] C. Taşaltın, T.A. Türkmen, N. Taşaltın, S. Karakuş, Highly sensitive non-enzymatic electrochemical glucose biosensor based on PANI: β12 borophene, J. Mater. Sci. Mater. Electron. vol. 32 (8) (2021) 10750–10760, https://doi.org/10.1007/S10854-021-05732-W.

[69] R.R. Mather, Surface modification of textiles by plasma treatments, Surf. Modif. Text. (2009) 296–317, https://doi.org/10.1533/9781845696689.296.

[70] X. Ji, et al., A novel top-down synthesis of ultrathin 2D boron nanosheets for multimodal imaging-guided cancer therapy, Adv. Mater. vol. 30 (36) (2018) 1803031, https://doi.org/10.1002/ADMA.201803031.

[71] S. Göktuna, N. Taşaltın, Preparation and characterization of PANI: α borophene electrode for supercapacitors, Phys. E Low-Dimens. Syst. Nanostruct. vol. 134 (2021), 114833, https://doi.org/10.1016/J.PHYSE.2021.114833.

[72] J.D. Clogston, A.K. Patri, Zeta potential measurement, Methods Mol. Biol. vol. 697 (2011) 63–70, https://doi.org/10.1007/978-1-60327-198-1_6/COVER.

[73] M. Farré, D. Barceló. Analysis and Risk of Nanomaterials in Environmental and Food Samples: Comprehensive Analytical Chemistry, 2012, p. 361.

[74] M. Nasrollahzadeh, M. Atarod, M. Sajjadi, S.M. Sajadi, Z. Issaabadi, Plant-mediated green synthesis of nanostructures: mechanisms, characterization, and applications, Interface Sci. Technol. vol. 28 (2019) 199–322, https://doi.org/10.1016/B978-0-12-813586-0.00006-7.

[75] G. Friedbacher, H. Fuchs, Classification of scanning probe microscopies (technical report), Pure Appl. Chem. vol. 71 (7) (1999) 1337–1357, https://doi.org/10.1351/pac199971071337.

[76] M.A.R. Laskar, et al., Formamidinium iodide for instantaneous and fluorescent detection of Pb2+ in water, J. Mater. Chem. C (2023).

[77] M.T. Rahman, M.S.A. Bhuiyan, M.J. Islam, K.M. Reza, A. Gurung, Q. Qiao, A flexible, ultrasensitive, and highly selective bi-functional acetone and ethanol gas sensor, in: Proceedings of the 12th International Conference on Electrical and Computer Engineering (ICECE), IEEE, 2022, pp. 84–87.

[78] E. Adhamash, et al., High-energy plasma activation of renewable carbon for enhanced capacitive performance of supercapacitor electrode, Electrochim. Acta vol. 362 (2020), 137148.

[79] D.J. Joshi, N.I. Malek, S.K. Kailasa, Borophene as a rising star in materials chemistry: synthesis, properties and applications in analytical science and energy devices, New J. Chem. vol. 46 (10) (2022) 4514–4533, https://doi.org/10.1039/D1NJ05271C.

[80] C. Hou, G. Tai, Y. Liu, X. Liu, Borophene gas sensor, Nano Res. vol. 15 (3) (2022) 2537–2544, https://doi.org/10.1007/S12274-021-3926-6/METRICS.

[81] C.S. Huang, A. Murat, V. Babar, E. Montes, U. Schwingenschlögl, Adsorption of the gas molecules NH3, NO, NO2, and CO on borophene, J. Phys. Chem. C vol.

122 (26) (2018) 14665–14670, https://doi.org/10.1021/ACS.JPCC.8B03811/ASSET/IMAGES/MEDIUM/JP-2018-03811H_0007.GIF.
[82] V. Shukla, J. Wärnå, N.K. Jena, A. Grigoriev, R. Ahuja, Toward the realization of 2D borophene based gas sensor, J. Phys. Chem. C vol. 121 (48) (2017) 26869–26876, https://doi.org/10.1021/ACS.JPCC.7B09552/SUPPL_FILE/JP7B09552_SI_001.PDF.
[83] C. Hou, G. Tai, B. Liu, Z. Wu, Y. Yin, Borophene-graphene heterostructure: preparation and ultrasensitive humidity sensing, Nano Res. vol. 14 (7) (2021) 2337–2344, https://doi.org/10.1007/S12274-020-3232-8/METRICS.
[84] C. Hou, G. Tai, Y. Liu, Z. Wu, Z. Wu, X. Liang, Ultrasensitive humidity sensing and the multifunctional applications of borophene–MoS2 heterostructures, J. Mater. Chem. A vol. 9 (22) (2021) 13100–13108, https://doi.org/10.1039/D1TA01940F.
[85] G. Brüllmann, K. Fritsch, R. Thurnheer, K.E. Bloch, Respiratory monitoring by inductive plethysmography in unrestrained subjects using position sensor-adjusted calibration, Respiration vol. 79 (2) (2010) 112–120, https://doi.org/10.1159/000212117.
[86] M.A. Dyachenko, et al., Sleep-related breathing disorders in patients with pulmonary arterial hypertension and chronic thromboembolic pulmonary hypertension, Arter. Hypertens. vol. 26 (1) (2020) 85–93, https://doi.org/10.18705/1607-419X-2020-26-1-85-93.
[87] M.W. Donnino, et al., Comparison between patients hospitalized with influenza and COVID-19 at a tertiary care center, J. Gen. Intern. Med. vol. 36 (6) (2021) 1689, https://doi.org/10.1007/S11606-021-06647-2.
[88] X. Tu, H. Xu, X. Wang, C. Li, G. Fan, X. Chu, First-principles study of pristine and Li-doped borophene as a candidate to detect and scavenge SO2 gas, Nanotechnology vol. 32 (32) (2021), 325502, https://doi.org/10.1088/1361-6528/ABFABC.
[89] Z. Yu, Y. Li, X. Yu, F. Chen, Computational study of borophene with line defects as sensors for nitrogen-containing gas molecules, ACS Appl. Nano Mater. vol. 3 (10) (2020) 9961–9968, https://doi.org/10.1021/ACSANM.0C01975/SUPPL_FILE/AN0C01975_SI_001.PDF.
[90] J. Li, X. Chen, Z. Yang, X. Liu, X. Zhang, Highly anisotropic gas sensing of atom-thin borophene: a first-principles study, J. Mater. Chem. C vol. 9 (3) (2021) 1069–1076, https://doi.org/10.1039/D0TC04691D.
[91] A. Omidvar, Borophene: a novel boron sheet with a hexagonal vacancy offering high sensitivity for hydrogen cyanide detection, Comput. Theor. Chem. vol. 1115 (2017) 179–184, https://doi.org/10.1016/J.COMPTC.2017.06.018.
[92] L.T. Ta, I. Hamada, Y. Morikawa, V.A. Dinh, Adsorption of toxic gases on borophene: surface deformation links to chemisorptions, RSC Adv. vol. 11 (30) (2021) 18279–18287, https://doi.org/10.1039/D1RA02738G.
[93] R. Bhuvaneswari, R. Chandiramouli, DFT investigation on the adsorption behavior of dimethyl and trimethyl amine molecules on borophene nanotube, Chem. Phys. Lett. vol. 701 (2018) 34–42, https://doi.org/10.1016/J.CPLETT.2018.04.032.
[94] Z. Wang, et al., Hole selective materials and device structures of heterojunction solar cells: recent assessment and future trends, APL Mater. vol. 7 (11) (2019), 110701, https://doi.org/10.1063/1.5121327.
[95] I.S. Karapınar, A.O. Pehlivan, A.E. Özsoy Özbay, A.U. Yazgan, N. Taşaltın, S. Karakuş, Improvement of the mechanical properties of cementitious composites by the novel synthesized borophene nanosheet, J. Compos. Mater. vol. 56 (10) (2022) 1615–1630, https://doi.org/10.1177/00219983221084771.
[96] C.H. Liu, Y.C. Chang, T.B. Norris, Z. Zhong, Graphene photodetectors with ultra-broadband and high responsivity at room temperature, Nat. Nanotechnol. vol. 9 (4) (2014) 273–278, https://doi.org/10.1038/nnano.2014.31.
[97] T. Ramanathan, et al., Functionalized graphene sheets for polymer nanocomposites, Nat. Nanotechnol. vol. 3 (6) (2008) 327–331, https://doi.org/10.1038/nnano.2008.96.
[98] B. Mortazavi, O. Rahaman, A. Dianat, T. Rabczuk, Mechanical responses of borophene sheets: a first-principles study, Phys. Chem. Chem. Phys. vol. 18 (39) (2016) 27405–27413, https://doi.org/10.1039/C6CP03828J.
[99] T. Someya, M. Amagai, Toward a new generation of smart skins, Nat. Biotechnol. vol. 37 (4) (2019) 382–388.
[100] C. Hou, G. Tai, Y. Liu, Z. Wu, X. Liang, X. Liu, Borophene-based materials for energy, sensors and information storage applications, Nano Res. Energy (2023).
[101] C. Hou, et al., Borophene pressure sensing for electronic skin and human-machine interface, Nano Energy vol. 97 (2022), 107189.
[102] H. Chand, A. Kumar, V. Krishnan, Borophene and boron-based nanosheets: recent advances in synthesis strategies and applications in the field of environment and energy, Adv. Mater. Interfaces vol. 8 (15) (2021) 2100045, https://doi.org/10.1002/ADMI.202100045.
[103] A. Mogulkoc, Y. Mogulkoc, D. Kecik, E. Durgun, The effect of strain and functionalization on the optical properties of borophene, Phys. Chem. Chem. Phys. vol. 20 (32) (2018) 21043–21050, https://doi.org/10.1039/C8CP03594F.
[104] C. Hou, G. Tai, Z. Wu, J. Hao, Borophene: current status, challenges and opportunities, ChemPlusChem vol. 85 (9) (2020) 2186–2196, https://doi.org/10.1002/CPLU.202000550.
[105] P. Ranjan, J.M. Lee, P. Kumar, A. Vinu, Borophene: new sensation in flatland, Adv. Mater. vol. 32 (34) (2020) 2000531, https://doi.org/10.1002/ADMA.202000531.
[106] M. Motlag, et al., Asymmetric 3D elastic–plastic strain-modulated electron energy structure in monolayer graphene by laser shocking, Adv. Mater. vol. 31 (19) (2019) 1900597, https://doi.org/10.1002/ADMA.201900597.
[107] Y. Duo, et al., Borophene-based biomedical applications: status and future challenges, Coord. Chem. Rev. vol. 427 (2021), 213549, https://doi.org/10.1016/J.CCR.2020.213549.

Arifur Rahman received Bachelor's in Mechanical Engineering from Chittagang University of Engineering & Technology, Bangladesh, in 2007 and currently is doing Master's in Mechanical Engineering from Dhaka University of Engineering & Technology, Bangladesh. His research interests include Advanced Materials, Engineering Tribology, 2D Materials, Nanomaterials, and Composite Materials. Besides, his research is focused on the synthesis and characterization of 2D materials including borophene.

Md Tawabur Rahman is an associate professor in the department of Electrical and Electronic Engineering at Khulna University of Engineering and Technology (KUET), Khulna, Bangladesh. He received Ph.D. in Electrical Engineering at South Dakota State University, USA. He received Bachelor's and Master's in Electrical and Electronic Engineering from KUET, Bangladesh. His research interests include electrochemical and chemical sensors for human health, environment, and agricultural applications. Besides, his research is focused on the synthesis and characterization of 2D materials including graphene, borophene, TMDCs, etc.

Mohammad Asaduzzaman Chowdhury is a professor of mechanical engineering at Dhaka University of Engineering and Technology (DUET), Gazipur, Bangladesh with about 23 years of teaching and research experiences. His research interests are engineering tribology, surface engineering, materials science and engineering, nanotechnology, 2D materials, energy, automation and robotics, coating technology, polymer and composite materials, and characterization of materials. He has published many research and review papers in refereed international journals and conference proceedings. He works as a consultant, advisor and expert member of many government and autonomous organizations, and is an editorial board member of many reputed international journals. He has also participated in international conferences as keynote speaker, session chair and advisory member.

Saad Bin Ekram received Bachelor's in Electrical and Electronic Engineering from Khulna University of Engineering & Technology, Bangladesh, in 2022 and is currently pursuing a Master's degree from the same university while working as a lecturer in EEE at Northern University Bangladesh. With a research focus on Perovskite Solar Cell Materials, Optical and Electronic Properties of 2D Materials, Nano-technology, and Renewable Energy, he is dedicated to advancing sustainable technologies and exploring innovative solutions for a greener future.

M.M. Kamal Uddin received Bachelor of Mechanical Engineering from Khulna University of Engineering & Technology, Bangladesh, in the Year 2003 and Masters of Applied Mechanics from ENSEM, Morocco in the Year 2011. He is studying Ph.D. in Mechanical Engineering at DUET, Gazipur. His research is focused on the synthesis and characterization of 2D materials including Borophene.

Md. Rasidul Islam is now working as a Departmental Chairman and Assistant Professor, Department of Electrical and Electronic Engineering, Department of Electrical and Electronic Engineering, Bangamata Sheikh Fojilatunnesa Mujib Science & Technology University, Jamalpur-2012, Bangladesh. He received his M.Sc. and B.Sc. in Electrical and Electronic Engineering degrees from Khulna University of Engineering and Technology, Khulna, Bangladesh. He got his Ph.D. from the Institute of Semiconductors, Chinese Academy of Sciences (CAS), Beijing, China. His research area consists of semiconductor materials (graphene, other 2D materials, perovskite materials) and devices (GFET, solar cell), computational physics, fabrication of perovskite solar cells and it's tandem solar cell, presently working on the physical properties of perovskite materials using density function theory method. Also, he is working on Li-ion battery.

Liang Dong is working as Vikram L. Dalal Professor in the department of Electrical and Computer Engineering (EpCE) at Iowa State University, IA, USA. He is also the director of Microelectronics Research Center (MRC) at ISU. He received Ph. D. in Electronic Science and Technology from Tsinghua University and B.S. in Precision Instrumentation (Mechano-electronic Engineering) from Xidian University. His research areas include Plant sensors, Environmental sensors, Agricultural sensors, Biomedical sensors, Sustainability, MEMS, Semiconductors, Nanotechnology, and Microoptics.